iScience

CellPress
OPEN ACCESS

Article

Dominant-negative HNF1α mutant promotes liver steatosis and inflammation by regulating hepatic complement factor D

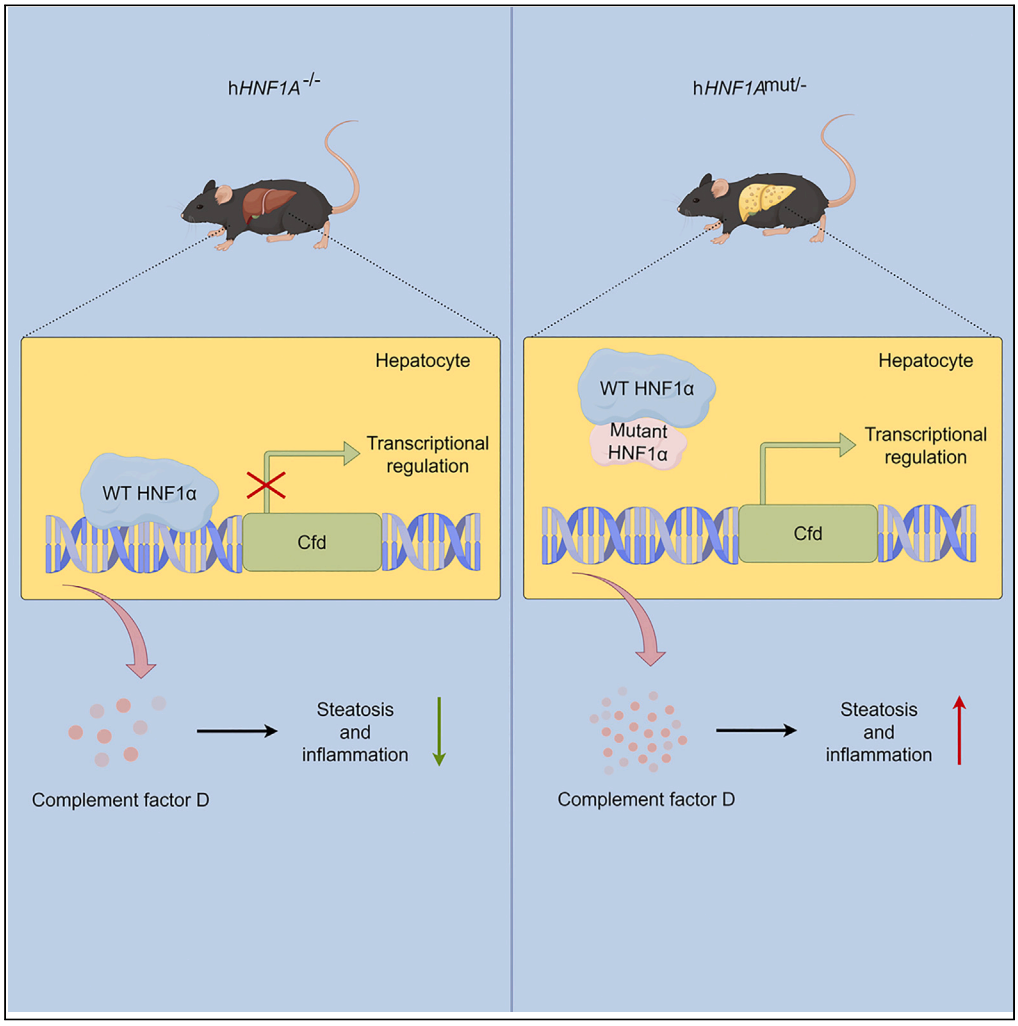

Moke Liu, Luna Liu, Honglin Guo, ..., Shanshan Shao, Jiajun Zhao, Peng Lu

shaoshanshan11@126.com (S.S.)
jjzhao@sdu.edu.cn (J.Z.)
sibslp@126.com (P.L.)

Highlights

Mice harboring HNF1α P291fsinsC mutation manifest hepatic steatosis and inflammation

HNF1α exerts negative regulation on Complement Factor D in hepatocytes

Inhibition of CFD mitigates intracellular glyceride accumulation in hepatocytes

Liu et al., iScience 26, 108018
October 20, 2023
https://doi.org/10.1016/j.isci.2023.108018

iScience

CellPress
OPEN ACCESS

Article

Dominant-negative HNF1α mutant promotes liver steatosis and inflammation by regulating hepatic complement factor D

Moke Liu,[1,2,3,4,5] Luna Liu,[2,3,4,5] Honglin Guo,[2] Xiude Fan,[2,3,4,5] Tianbao Liu,[2,3,4,5] Chao Xu,[2,3,4,5] Zhao He,[2,3,4,5] Yongfeng Song,[2,3,4,5] Ling Gao,[2,3,4,5] Shanshan Shao,[2,3,4,5,*] Jiajun Zhao,[2,3,4,5,*] and Peng Lu[1,2,3,4,6,2,*]

SUMMARY

Patients with *HNF1A* variants may develop liver steatosis, while the underlying mechanism is still unclear. Here, we established a mouse model carrying the dominant-negative HNF1α P291fsinsC mutation (h*HNF1A*$^{mut/-}$) and found that the mutant mice developed liver steatosis spontaneously under the normal chow diet. Transcriptome analysis showed significant upregulation of *Cfd* and other genes related to innate immune response in the liver of h*HNF1A*$^{mut/-}$ mice. The changes in lipid metabolism and complement pathways were also confirmed by proteomics. We demonstrated that HNF1α inhibited CFD expression in hepatocytes, and the P291fsinsC mutant could reverse this inhibitory effect. Furthermore, the suppression of CFD with specific inhibitor or siRNAs reduced triglyceride levels in hepatocytes, suggesting that CFD regulated hepatocyte lipid deposition. Our results demonstrate that the HNF1α P291fsinsC mutant promotes hepatic steatosis and inflammation by upregulating CFD expression, and targeting CFD may delay the progression of nonalcoholic fatty liver disease.

INTRODUCTION

Nonalcoholic fatty liver disease (NAFLD) is a pathological condition characterized by the excessive accumulation of fat in the liver, which results in systemic metabolic abnormalities and an increased risk of non-alcoholic steatohepatitis (NASH), cirrhosis, and hepatocellular carcinoma.[1] Increasing evidences indicate that the development of NAFLD is a result of synergistic effects of various factors, including genetic susceptibility and environmental stimuli.[2] Despite the strong association between obesity and NAFLD, recent studies show that even lean individuals can suffer from this condition.[3] Therefore, gaining an understanding of NAFLD-related genes and polymorphisms could provide further insight into its etiology.

HNF1α (hepatocyte nuclear factor 1 homeobox α), encoded by *HNF1A*, was first identified in the hepatocyte. It is also widely distributed in other tissues, including the pancreas, gastrointestinal tract, and kidney.[4] The gene *HNF1A* is composed of ten exons, encoding a transcription factor of 631-amino acid protein that contains three functional domains: an N-terminal dimerization domain (1–32), a homeobox DNA binding domain (82–281) and a transactivation domain (282–631).[5] HNF1α plays a critical role in controlling the expression of many liver-specific genes.[6] It is essential for the differentiation of hepatocytes and the maintenance of normal liver function. It has been reported that individuals with *HNF1A* variants are prone to developing steatosis-associated hepatocellular adenoma.[7–9] This is also observed in *Hnf1a* knockout mice, which exhibit hepatomegaly and fatty liver.[10] These findings indicate that *HNF1A* plays an important role in maintaining liver lipid homeostasis. Since the target genes of *HNF1A* are involved in the regulation of glucose and lipid metabolism and immune response, the regulatory networks centered around *HNF1A* are complex and abstrusity.[11,12] Despite several studies having made an effort to explore the role of HNF1α in the pathogenesis of liver steatosis,[13–15] the underlying molecular mechanism still cannot be fully explained. To obtain functional data on genetic mutations *in vivo*, animal models with point mutation are frequently utilized to simulate human disease.[16–18] To date, over 1000 variants spanning from the promoter to the 3′UTR region have been identified in the *HNF1A* gene.[5] Although certain mutations have been employed to access the impact of *HNF1A* in other tissues,[19,20] there is currently a paucity of models carrying functional mutations to investigate the role of *HNF1A* in the liver.

[1]Department of Endocrinology, Shandong Provincial Hospital, Shandong University, Jinan 250021, China
[2]Key Laboratory of Endocrine Glucose & Lipids Metabolism and Brain Aging, Ministry of Education, Department of Endocrinology, Shandong Provincial Hospital Affiliated to Shandong First Medical University, Jinan, Shandong 250021, China
[3]Shandong Key Laboratory of Endocrinology and Lipid Metabolism, Jinan 250021, China
[4]Shandong Institute of Endocrine and Metabolic Diseases, Jinan 250021, China
[5]Shandong Engineering Research Center of Stem Cell and Gene Therapy for Endocrine and Metabolic Diseases, Jinan 250021, China
[6]Lead contact
*Correspondence: shaoshanshan11@126.com (S.S.), jjzhao@sdu.edu.cn (J.Z.), sibslp@126.com (P.L.)
https://doi.org/10.1016/j.isci.2023.108018

The phased progression of NAFLD is often accompanied by an enhanced inflammatory response. Adipocyte-derived Monocyte chemoattractant protein-1 (MCP-1) has been shown to promote hepatic insulin resistance and steatosis, and MCP-1 deficient mice are protected from diet-induced hepatic steatosis even though they still develop obese.[21] It suggests that NAFLD could be initiated by the innate immune system. The complement system is a part of the innate immune system.[22] The majority of complement components are synthesized in the liver and secreted into the bloodstream to exert their effects.[23] Upon different stimuli, the complement system can be activated via three different pathways, including the classical, alternative, and lectin pathways. Activation of these pathways leads to the cleavage of complement component 3 (C3) and complement component 5 (C5) to form the membrane attack complex and subsequent cell lysis.[24] Previous clinical studies have found that uncontrolled activation of the complement system is associated with the development of NAFLD.[25,26] The intervention on complement pathways protected the liver from lipid accumulation and inflammation.[27] Additionally, HNF1α regulates the complement system through controlling the transcription of complement component 4 binding protein A (*C4BPA*), complement component 5 (*C5*) and complement component 8 A (*C8A*).[28,29] However, the regulation of other complement genes by HNF1α, especially in the context of NAFLD, is not fully understood.

Based on the above questions, we constructed a mouse model carrying a human dominant-negative HNF1α P291fsinsC mutant to explore how the pathogenic mutant affected lipid metabolism. Comprehensive multiomics analysis and biochemical experiments were carried out to reveal the potential mechanisms promoting hepatic steatosis and inflammation. Collectively, our findings suggest that the dominant-negative HNF1α mutant promotes the onset of liver steatosis and inflammation. HNF1α has the capacity to modulate the expression of complement factor D within hepatocytes. The exacerbated lipid accumulation resulting from the HNF1α P291fsinsC mutation might be ameliorated via the targeted inhibition of CFD. Our study unveils a novel mechanism by which HNF1α governs hepatic lipid metabolism.

RESULTS

Generation of human HNF1α P291fsinsC mutation knock-in mice

HNF1α P291fsinsC is a frameshift mutation that occurs adjacent to the transactivation domain, resulting in the production of a truncated protein consisting of only 315 amino acids (Figure S1A). In normal conditions, the wild-type (WT) HNF1α forms a homodimer to facilitate binding to the promoter regions of target genes and initiate the transcriptional process. However, upon the emergence of HNF1α P291fsinsC, it can bind with WT HNF1α to form a heterodimer, thereby exerting a dominant-negative effect. This mutation is known to be a hotspot in Europe and America and is frequently observed in patients with both Maturity Onset Diabetes of the Young (MODY) 3 and steatosis-associated hepatocellular adenoma.[30–32] To explore the impact of HNF1α on NAFLD, we constructed a hHNF1α P291fsinsC flox mice by introducing a *CAG*-LSL-*HNF1A* mutant CDS (with P291fsinsC mutation)-polyA segment into H11 locus on C57BL/6J genetic background. Heterozygous hHNF1α P291fsinsC mutant (h*HNF1A*$^{mut/-}$) mice were generated through a cross between hHNF1α P291fsinsC flox mice and *Cag*-cre mice (Figure 1A), and their littermates (h*HNF1A*$^{-/-}$) were used as control mice. It was difficult to obtain homozygous h*HNF1A*$^{mut/mut}$ mice, indicating that the inserted HNF1α P291fsinsC mutant may cause embryonic lethality.

Although the male h*HNF1A*$^{mut/-}$ mice had a shorter body length and lower body weight compared to the h*HNF1A*$^{-/-}$ mice (Figures 1B and 1C), the levels of growth hormone and serum insulin-like growth factor 1 (IGF-1) were found to be similar between the two groups (Figures S1B and S1C). The truncated mutant protein was detected in the liver of h*HNF1A*$^{mut/-}$ mice (Figure 1D). Besides, we also examined the mRNA level of the inserted hHNF1α P291fsinsC mutant in the various organs and tissues (Figure S1D). To assess the potential dominant-negative impact of the introduced P291fsinsC mutant, we conducted an analysis of HNF1α protein expression within the liver. Our investigation revealed a shift in the cellular localization of HNF1α, transitioning from predominantly nucleus to a distribution spanning both the nucleus and cytoplasm (Figure 1E). Notably, in the livers of h*HNF1A*$^{mut/-}$ mice, the mRNA levels of *Hgfac*, *Pklr*, and *Slc2a2*—known target genes of *Hnf1a*—exhibited a substantial reduction, as demonstrated in Figure 1F. To assess the ability of glucose fluctuation response in h*HNF1A*$^{mut/-}$ mice, the glucose tolerance test (GTT) and insulin tolerance test (ITT) were performed. It turned out that the h*HNF1A*$^{mut/-}$ mice exhibited some degree of impaired insulin sensitivity, but their glucose disposal performance was better than that of their control littermates (Figures S1E and S1F). These findings suggested that the human HNF1α P291fsinsC mutant was successfully integrated in mice and had certain adverse effects on their development.

Overexpression of h*HNF1A* mutant induced disorders of lipid metabolism and hepatic steatosis

Despite exhibiting lower body weight and normal glucose response compared to their littermates, h*HNF1A*$^{mut/-}$ mice showed higher serum triglyceride and cholesterol levels when fed with a normal chow diet. The levels of total triglyceride (TG), total cholesterol (TC), low-density lipoprotein (LDL) and high-density lipoprotein (HDL) were all dramatically increased compared with the control group (Table 1). Meanwhile, the alanine transaminase (ALT) and aspartate aminotransferase (AST) levels were increased to 2- and 1.5-times as much as that of the control group (Table 1), indicating the presence of liver damage in h*HNF1A*$^{mut/-}$ mice. Next, we examined the effects of the hHNF1α P291fsinsC mutant on the mice liver. The hepatomegaly of the mutant mice was detected, and the liver-to-body weight ratio was markedly higher than that of their littermates (Figures 2A and 2B). In addition, the hepatocellular ballooning and fat accumulation could be observed in the mutant mice, which was confirmed by hematoxylin and eosin (H&E) staining and oil red staining. These phenotypes were continuous from 10 weeks to 40 weeks (Figure 2C and S2A).

Consistent with the histological changes, the corresponding hepatic TG content of the mutant mice was also increased twice as much as that in control group (h*HNF1A*$^{-/-}$ group 158.6 ± 19.91 nmol/mg, h*HNF1A*$^{mut/-}$ group 299.3 ± 28.88 nmol/mg, p value < 0.01). There were no significant differences in the TC and free cholesterol (FC) contents between the two groups (TC, h*HNF1A*$^{-/-}$ group 6.243 ± 0.98 nmol/mg,

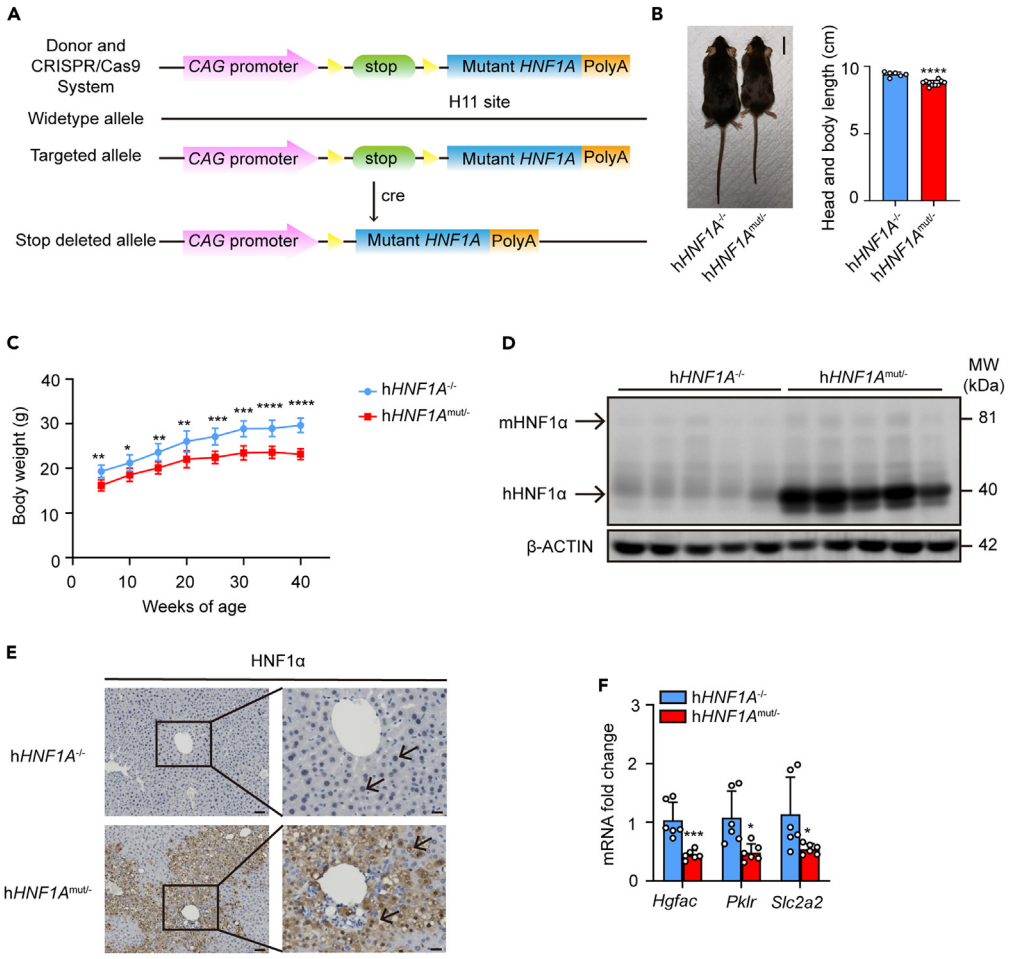

Figure 1. General phenotypic analysis of h*HNF1A*$^{mut/-}$ mice

(A) Establishment strategy of h*HNF1A*$^{mut/-}$ mice.

(B) A representative photograph of 40-week-old h*HNF1A*$^{-/-}$ (left) and h*HNF1A*$^{mut/-}$ (right) mice. Scale bar: 2 cm. The head and body length of two groups were measured (n = 6 for h*HNF1A*$^{-/-}$ group, n = 10 for h*HNF1A*$^{mut/-}$ group).

(C) Body weight curve of male h*HNF1A*$^{-/-}$ and h*HNF1A*$^{mut/-}$ mice under normal chow diet (n = 5 for h*HNF1A*$^{-/-}$ group, n = 8 for h*HNF1A*$^{mut/-}$ group).

(D) Protein levels of human and mouse hepatocyte nuclear factor 1 alpha (HNF1α) in the livers of h*HNF1A*$^{-/-}$ and h*HNF1A*$^{mut/-}$ mice (n = 5 for each group).

(E) Immunohistochemistry staining of HNF1α in the livers of h*HNF1A*$^{-/-}$ and h*HNF1A*$^{mut/-}$ mice. Scale bar, left: 50 μm, right: 20 μm. Arrows mark the cell localization of the HNF1α (n = 3 for each group).

(F) mRNA levels of *Hnf1a* target genes, *Hgfac*, *Pklr* and *Slc2a2* (n = 6 for each group). All data are presented as mean ± SD. *p < 0.05; **p < 0.01; ***p < 0.001; ****p < 0.0001 by an unpaired two-tailed t test. See also Figure S1.

h*HNF1A*$^{mut/-}$ group 9.153 ± 1.24 nmol/mg FC, h*HNF1A*$^{-/-}$ group 4.704 ± 0.92 nmol/mg, h*HNF1A*$^{mut/-}$ group 5.887 ± 1.16 nmol/mg) (Figures 2D–2F). The elevation of hepatic TG levels was also detected in the 10w- and 40w-old mice (Figures S2B–S2G). Next, we examined the expression of genes involved in lipogenesis. As depicted in Figure 2G, the protein expression of fatty acid synthase (FASN), a key enzyme involved in *de novo* lipogenesis, was notably increased in the liver of the mutant mice, whereas the expression of sterol regulatory element binding protein 1 (SREBP-1C) and stearoyl-coenzyme A desaturase 1(SCD1) were remained unchanged. Regarding the genes related to fatty acid uptake, it was found that peroxisome proliferator activated receptor gamma (Pparγ) and CD36 were upregulated at the transcriptional level, while their protein levels were not changed (Figure S2). These results indicated that the inactivation of HNF1α induced hepatomegaly, ectopic fat accumulation and liver damage in the mutant mice.

Multiomics analysis revealed the molecular changes in the liver of h*HNF1A*$^{mut/-}$ mice

To identify potential factors involved in the spontaneous development of liver steatosis, we performed bulk RNA-seq analysis screening the differential expressed genes (DEGs) between the h*HNF1A*$^{-/-}$ and h*HNF1A*$^{mut/-}$ groups. In general, there were tremendous differences in gene expression as shown in the heatmap (Figure S3A). Of the DEGs identified, 481 were upregulated and 190 were downregulated (padj<=0.05, |log2FoldChange|≥1) between the two groups (Figure 3A). The expression of TOP upregulated genes was investigated.

Table 1. Serum chemistry of 20-week-old h*HNF1A*$^{mut/-}$ mice

	levels in mice		
Component	h*HNF1A*$^{-/-}$	h*HNF1A*$^{mut/-}$	p value
ALT (U/L)	54.64 ± 8.13	106.30 ± 32.86	0.006**
AST (U/L)	162.40 ± 24.47	236.5 ± 54.28	0.016*
TG (mmol/L)	0.68 ± 0.11	0.82 ± 0.09	0.025*
LDL-C (mmol/L)	0.17 ± 0.01	0.34 ± 0.13	0.013*
HDL-C (mmol/L)	2.04 ± 0.13	2.92 ± 0.56	0.006**
TC (mmol/L)	2.33 ± 0.12	3.50 ± 0.70	0.004**

Serum was collected from mice of h*HNF1A*$^{-/-}$ and h*HNF1A*$^{mut/-}$ at 20-week-age and subjected to analysis for levels of alanine transaminase (ALT), aspartate aminotransferase (AST), triglyceride (TG), low density lipoprotein (LDL-C), high-density lipoprotein (HDL-C) and total cholesterol (TC). Values are presented as mean ± S.D. (n = 5 for h*HNF1A*$^{-/-}$ group, n = 8 for h*HNF1A*$^{mut/-}$ group). The data were analyzed by one-way ANOVA with post-hoc comparisons. A value of $p < 0.05$ was considered to be statistically significant. *$p < 0.05$; **$p < 0.01$.

Complement factor D (*Cfd*), D site albumin promoter binding protein (*Dbp*), neurotrophic receptor tyrosine kinase 2 (*Ntrk2*), orosomucoid 3 (*Orm3*), subfamily b, polypeptide 9 (*Cyp2b9*) and syndecan binding protein 2 (*Sdcbp2*) had significant differences between two groups (Figure 3B). As for downregulated genes, the cytochrome P450, family 2, subfamily d, polypeptide 9 (*Cyp2d9*), glutathione S-transferase, pi 1 (*Gstp1*), fatty acid binding protein 1 (*Fabp1*) and acyl-CoA synthetase long-chain family member 1 (*Acsl1*) were also significantly decreased in the liver of h*HNF1A*$^{mut/-}$ group (Figure S3B). Gene Ontology (GO) analysis showed that the upregulated DEGs were primarily associated with the innate immune response, suggesting that hepatic steatosis was accompanied by inflammation changes in h*HNF1A*$^{mut/-}$ mice (Figure 3C). To further investigate how molecular pathways were affected at the protein level, a proteomic analysis was performed. The proteome profiling discovered 34945 peptides and 5792 proteins (Figure S3C). Of these proteins, 129 were upregulated and 93 were downregulated in the liver of h*HNF1A*$^{mut/-}$ mice ($p<=0.05$, $|\text{FoldChange}| \geq 1.3$) (Figure S3D). To gain further understanding the signaling pathways related to the differentially expressed proteins, 222 differential expressed proteins were mapped to the GO and Kyoto Encyclopedia of Genes and Genomes (KEGG) databases. As shown in Figure 4A, the upregulated proteins were mainly involved in lipid metabolism and blood coagulation in GO analysis. Consistently, the KEGG analysis also showed that the complement and coagulation cascades were significantly altered in the upregulated pathways (Figure 4B). Complement and coagulation are evolutionarily related proteolytic cascades in the blood that are critical for innate response to injury. Given the significant changes in innate immune response in the transcriptome analysis, we hypothesized that the human HNF1α P291fsinsC mutant may be involved in the activation of the complement system, which has been reported to be associated with the development of hepatic fat accumulation and inflammation.

Complement factor D and alternative complement pathway were stimulated in the livers of h*HNF1A*$^{mut/-}$ mice

To investigate the molecular changes in the complement system, we initially assessed the expression of genes involved in the three complement pathways using QPCR. The results showed that the classical pathway (complement component 1, q subcomponent (*C1q*), *C5*), Mannose-binding lectin pathway (MBL-associated serine protease 2 (*Masp2*)) and alternative pathway (*Cfd*) were stimulated in the liver of h*HNF1A*$^{mut/-}$ mice (Figure 5A). Consistent with the result of transcriptome analysis, the upregulation of *Cfd*, which encodes complement factor D, was particularly prominent among the genes involved in the complement system. Moreover, the protein levels of hepatic CFD, serum CFD, and its catalytic product complement component 3a (C3a) were also significantly raised in h*HNF1A*$^{mut/-}$ mice (Figures 5B–5D). We further evaluate the extent of hepatic inflammation in h*HNF1A*$^{-/-}$ and h*HNF1A*$^{mut/-}$ mice. The expression of macrophage marker genes (integrin alpha M (*Cd11b*), integrin alpha X (*Cd11c*), adhesion G protein-coupled receptor E1 (*F4/80*), lectin, galactose binding, soluble 3 (*Mac2*)), chemokine (C-C motif chemokine ligand 2 (*Ccl2*)) and NK cell marker gene (killer cell lectin-like receptor subfamily B member 1C (*Nk1.1*)) were significantly upregulated (Figure 5E), while the expression of tumor necrosis factor alpha (*Tnfα*), interleukin 1 beta (*Il-1β*) and interleukin 6 (*Il-6*) were not affected (Figure S4A). Since CFD was reported to be highly expressed in adipose tissues, the mRNA level of *Cfd* in adipose tissue was examined and there was no difference between two groups (Figure S4B). These results suggested that CFD was abnormally expressed in the liver of h*HNF1A*$^{mut/-}$ mice, accompanied by complement system activation and increased immune response.

HNF1α negatively regulated complement factor D expression in hepatocyte

To explore the mechanism behind the abnormal expression of CFD in the liver of h*HNF1A*$^{mut/-}$ mice, we transfected the wild-type (WT) *HNF1A* into HepG2 cells and found that the *CFD* mRNA level was inhibited (Figure 6A). Furthermore, the knockdown of mouse *Hnf1a* in AML12 cells using siRNAs dramatically enhanced the expression of *Cfd*, as shown in Figure 6B. To further confirm the negative regulatory effect of HNF1α on CFD expression, we performed *Hnf1a* knockdown in high-fat diet mice by tail vein injection of AAV-shRNA in the liver. Consistent with our findings in h*HNF1A*$^{mut/-}$ mice, the protein expressions of CFD, FASN, and PPARγ in livers of high-fat diet HFD-shHNF1α mice were notably increased, whereas SREBP-1C, SCD1, and CD36 were at the similar levels with HFD-NC mice (Figure S5). Based on these findings, we were prompted to investigate whether HNF1α directly regulated the transcription of *CFD*. To address this question, a luciferase reporter plasmid

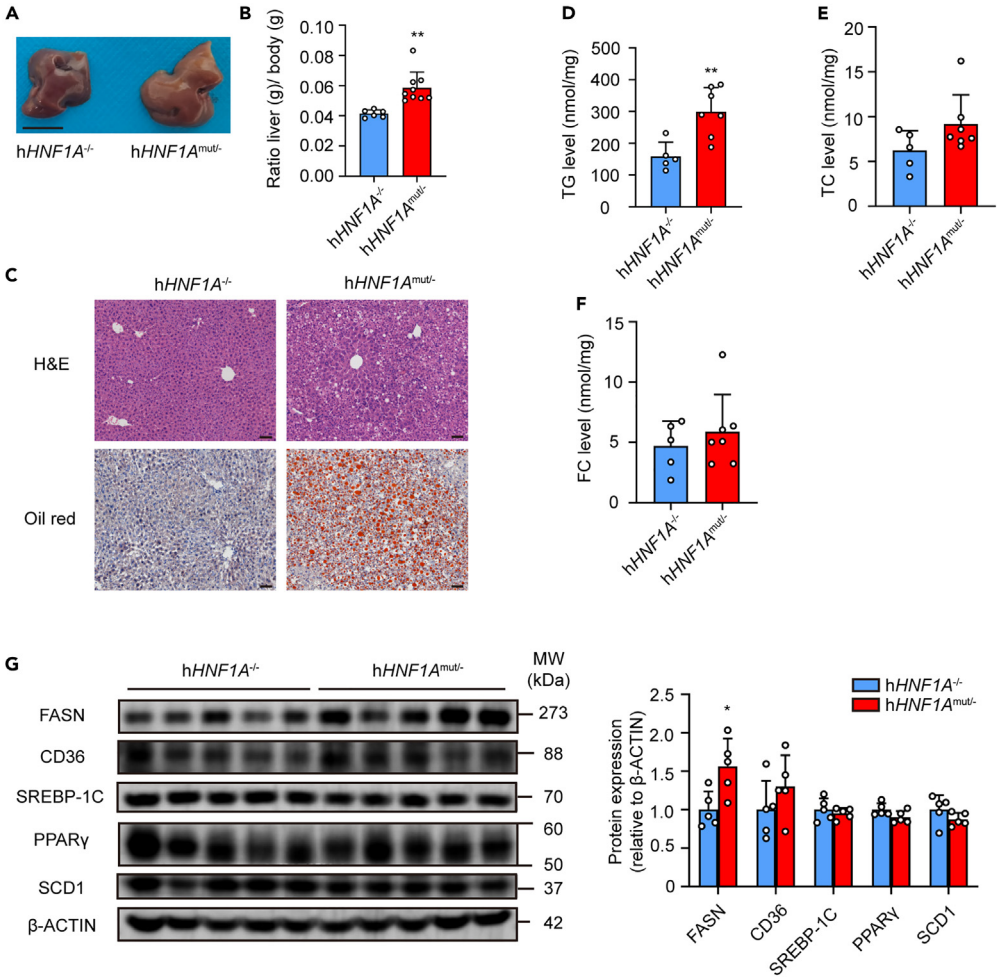

Figure 2. h*HNF1A*$^{mut/-}$ mice developed hepatomegaly, lipid accumulation in liver

(A) Representative images of livers of 20-week-old male mice. Scale bar: 1 cm.

(B) Ratio of liver weight to body weight (n = 6 for h*HNF1A*$^{-/-}$ group, n = 9 for h*HNF1A*$^{mut/-}$ group).

(C) Representative images of Hematoxylin and eosin (H&E) staining, Oil red staining of livers of 20-week-old male mice. Scale bar: 50μm.

(D–F) Levels of triglyceride (TG) (D), total cholesterol (TC) (E) and free cholesterol (FC) (F) in livers of 20-week-old male mice (n = 5 for h*HNF1A*$^{-/-}$ group, n = 7 for h*HNF1A*$^{mut/-}$ group).

(G) Protein levels of fatty acid synthase (FASN), sterol regulatory element binding protein 1 (SREBP-1C), CD36 molecule (CD36), peroxisome proliferator activated receptor gamma (PPARγ), stearoyl-coenzyme A desaturase 1 (SCD1) and β-ACTIN expressions in livers of h*HNF1A*$^{-/-}$ and h*HNF1A*$^{mut/-}$ mice (n = 5 for each group). All data are presented as mean ± SD. *p < 0.05; **p < 0.01 by an unpaired two-tailed t test. See also Figures S2 and S8.

was constructed containing approximately 1000bp upstream from the transcription start site of human *CFD* promoter. It demonstrated that with the increasing amounts of WT *HNF1A* plasmids, the relative activity of the *CFD* promoter was decreased (Figure 6C). Furthermore, when the cells were transfected with WT *HNF1A* or P291fsinsC mutant plasmids, along with the human *CFD* promoter luciferase reporter, the luciferase activity was reduced by the wide-type *HNF1A* to only 35% of normal conditions. On the contrary, P291fsinsC mutant abolished this inhibitory effect and promoted the luciferase activity to about 120% of normal reporter activity (Figure 6D).

To elucidate the *CFD* promoter region regulated by HNF1α, we generated *CFD* promoter fragments with varying lengths, guided by the conservation of promoter sequences across different species (Figure S6). As shown in Figure 6E, within the −1000/+26 bp promoter fragment, HNF1α exhibited its most potent inhibitory effect on the promoter. Upon the deletion of the sequence spanning from −1000bp to −486bp, while HNF1α continued to exert a certain level of inhibitory impact on the *CFD* promoter, the strength of inhibition was noticeably weaker than that observed in the −1000/+26 bp promoter fragment. To further investigate this interaction, we conducted chromatin immunoprecipitation (ChIP) assays. In HepG2 cells overexpressing wild-type HNF1α, we employed anti-Flag antibody to enrich the chromatin complex. We identified a sequence ranging from −1000bp to −821bp within the *CFD* promoter that could be amplified by PCR (Figure 6F). These results suggested that HNF1α exerts a negative regulatory effect on *CFD* expression at the transcription level.

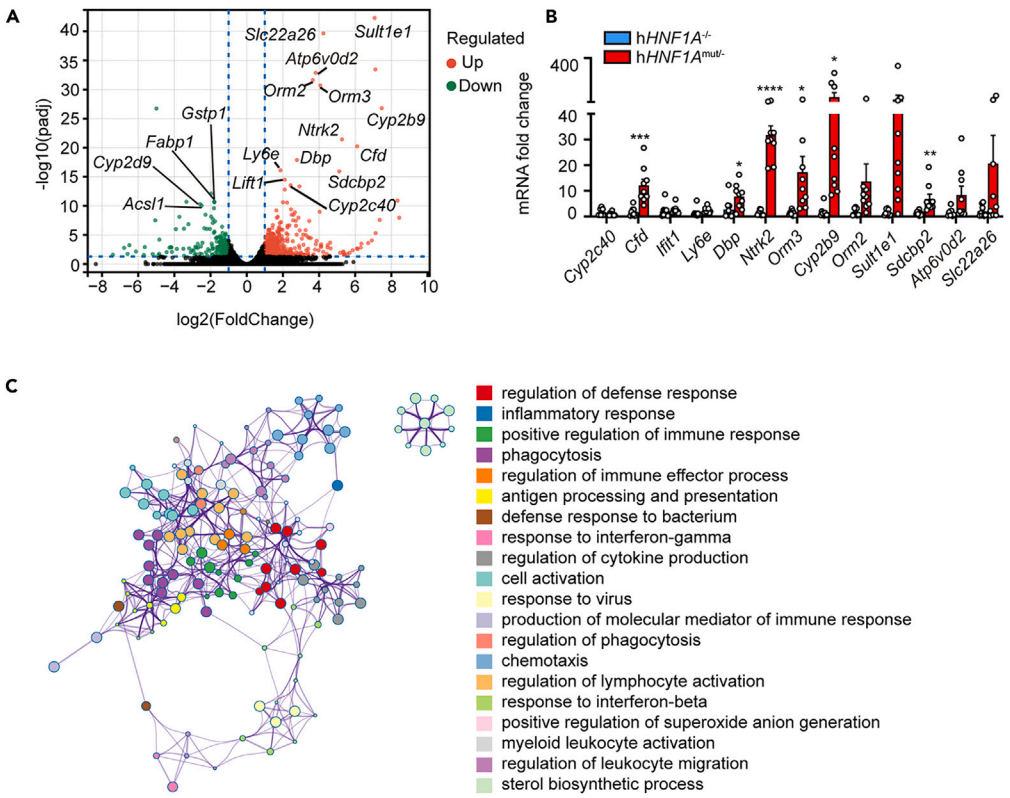

Figure 3. Transcriptome analysis of h*HNF1A*$^{mut/-}$ vs. h*HNF1A*$^{-/-}$ mice

(A) Volcano map of transcriptome analysis of livers of 40-week-old male mice (padj<=0.05, |log2FoldChange>=1) (n = 3 for each group). The TOP upregulated or downregulated genes were labeled.

(B) mRNA levels of TOP differential expressed genes (DEG) from transcriptome analysis in liver. (n = 9 for each group). Data are shown by mean ± SD. *p < 0.05; **p < 0.01; ***p < 0.001; ****p < 0.0001 by an unpaired two-tailed t test.

(C) Networks of enriched terms across upregulated gene expressions in transcriptome analysis (padj <0.01). See also Figure S3.

HNF1A inversely correlated with complement factor D in patients with nonalcoholic fatty liver disease but not in non-nonalcoholic fatty liver disease individuals

It is interesting to ask that whether the negative regulation of HNF1α on CFD that we observed in our model also exists in human liver. To investigate this, we analyzed the correlation between the expression of *HNF1A* and several genes involved in the three different complement pathways in liver samples obtained from 80 patients with NAFLD of GSE159088 and 464 non-NAFLD individuals of GSE25935. In agreement with the results gained in mice, *HNF1A* was inversely correlated with *CFD* and *C1Q*, which represent alternative and classic complement pathways, respectively, in patients with NAFLD. However, this correlation was not observed in non-NAFLD individuals (Table S1). Additionally, we did not observe any correlations between *HNF1A* and genes involved in the mannose-binding lectin pathway in patients with NAFLD (Figure S7A). We also investigated the correlation between *HNF1A*, *CFD* and certain genes involved in lipid metabolism (Figure S7B) and inflammation (Figure S5C). The results showed that *HNF1A* had an inverse correlation with *IL1B*, *CCL2* and C-X-C motif chemokine ligand 1 (*CXCL1*), while *CFD* had a positive correlation with *PPARG* and *CD36* genes, which was basically consistent with the findings in mouse model.

Triglyceride accumulation was attenuated through either HNF1α overexpression or complement factor D inhibition in hepatocyte

According to previous studies, the deficiency of HNF1α could increase the HFD-induced lipid accumulation in the liver, whereas the deletion of *Cfd* could attenuate it.[27,33] To determine these effects, we overexpressed wide-type or P291fsinsC mutant HNF1α, and used a selective small-molecule inhibitor against complement factor D (ACH-4471) in HepG2 cells pretreated with free fatty acid (FFA). ACH-4471 could potently inhibit the proteolytic activity of complement factor D, and is currently undergoing phase 2 clinical trials for the treatment of paroxysmal nocturnal hemoglobinuria (PNH) and atypical hemolytic syndrome (aHUS).[34] As depicted in Figure 7A, the overexpression of HNF1α exhibited a significant capacity to impede the accumulation of triglycerides induced by FFA. Conversely, the overexpression of the HNF1α P291fsinsC mutant exacerbated triglyceride deposition. To assess the impact of ACH-4471 on hepatocytes harboring the HNF1α P291fsinsC mutation, we introduced ACH-4471 to HepG2 cells pre-treated with FFA and transfected with P291fsinsC plasmids. Notably, this intervention led to a discernible reduction in elevated triglyceride levels, as demonstrated in Figure 7B. To extend these findings, we

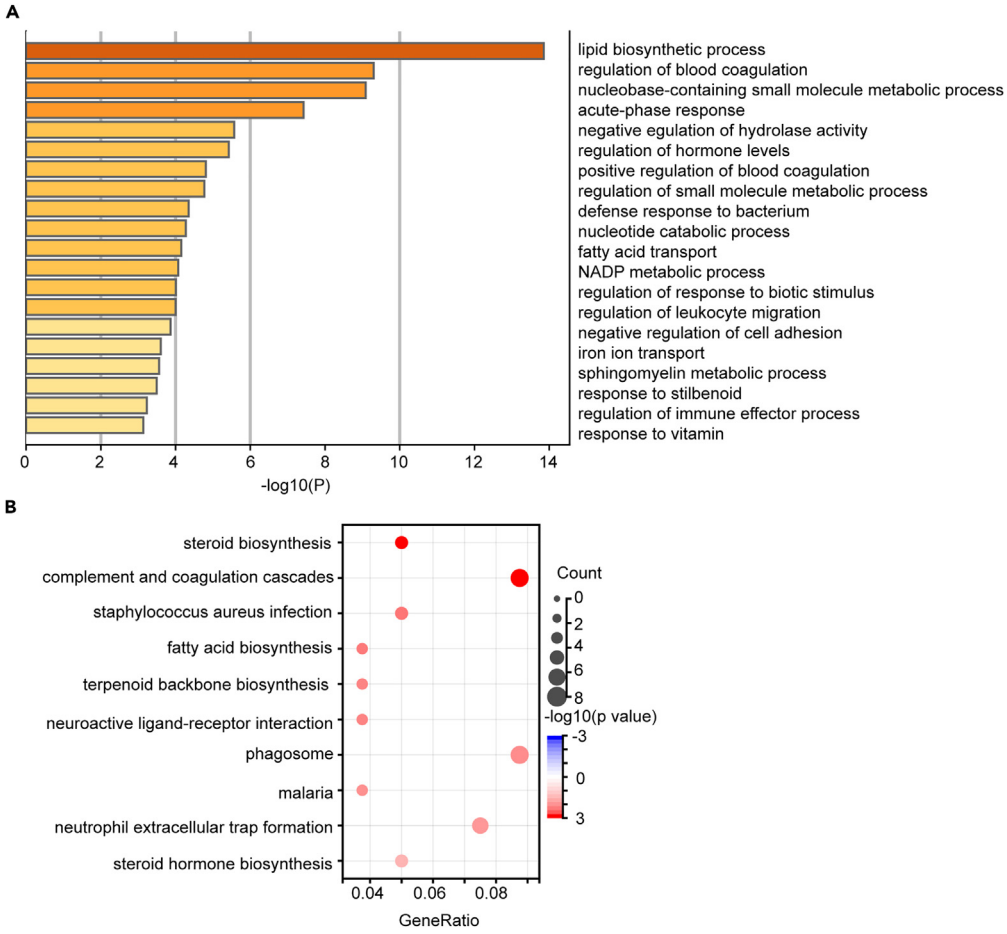

Figure 4. Proteome analysis of h*HNF1A*$^{mut/-}$ vs. h*HNF1A*$^{-/-}$ mice

(A) TOP 20 upregulated biological processes analyzed by Gene Ontology (GO) in proteome analysis.

(B) Kyoto Encyclopedia of Genes and Genomes (KEGG) analysis of upregulated pathways in proteome profiling (≥1.3-fold, p value<=0.05). See also Figure S3.

sought to confirm the effect of CFD inhibition on primary hepatocytes isolated from h*HNF1A*$^{mut/-}$ mice. To achieve this, we evaluated the efficacy of three distinct mouse *Cfd* siRNAs (si*Cfd*s). As displayed in Figure 7C, si*Cfd*1 and si*Cfd*2 both demonstrated notable reductions in *Cfd* transcription levels. This downregulation translated into diminished triglyceride content within primary hepatocytes upon transfection with si*Cfd*1 and si*Cfd*2, as illustrated in Figure 7D. Specifically, among the transcription levels of key genes implicated in *de novo* lipogenesis, only *Fasn* was significantly suppressed by both si*Cfd*1 and si*Cfd*2. Intriguingly, among the three groups, the mRNA levels of genes associated with fatty acid uptake—*Pparg*, *Cd36*, and *Fatp2*—displayed no discernible changes, as depicted in Figure 7E. These results indicated that upregulating the expression of HNF1α or inhibiting the proteolytic activity of CFD could ameliorate hepatic lipid accumulation induced by the HNF1α P291fsinsC mutant.

DISCUSSION

In this study, we constructed a mouse model expressing the dominant-negative human HNF1α P291fsinsC mutant globally. Our results showed that the h*HNF1A*$^{mut/-}$ mice exhibited elevated serum TG concentrations, hepatic lipid accumulation, and inflammation. We performed transcriptome and proteome analysis to explore the molecular alterations induced by the dominant-negative mutation. CFD, a crucial protease that triggers the alternative complement pathway, was found to abnormally expressed in the liver of h*HNF1A*$^{mut/-}$ mice. We demonstrate that HNF1α suppresses the expression of CFD in hepatocytes, while the dominant-negative HNF1α mutant could alleviate the inhibitory effect on CFD. These results indicate that the abnormal CFD expression induced by human HNF1α P291fsinsC mutant may be involved in liver steatosis and inflammation.

HNF1A is the genetic cause of several metabolic disorders, such as MODY3, Hyperinsulinaemic hypoglycaemia (HH), hepatocellular adenoma and HCC.[5,35–37] Although most studies about *HNF1A* have focused on the disorders of glucose metabolism, the hepatic lipid metabolism of patients with *HNF1A* variants does not draw sufficient attention. MODY3 is the most prevalent disorder caused by mutations in the *HNF1A* gene. However, patients with MODY3 typically do not exhibit other clinical features prior to the onset of hyperglycemia. They are

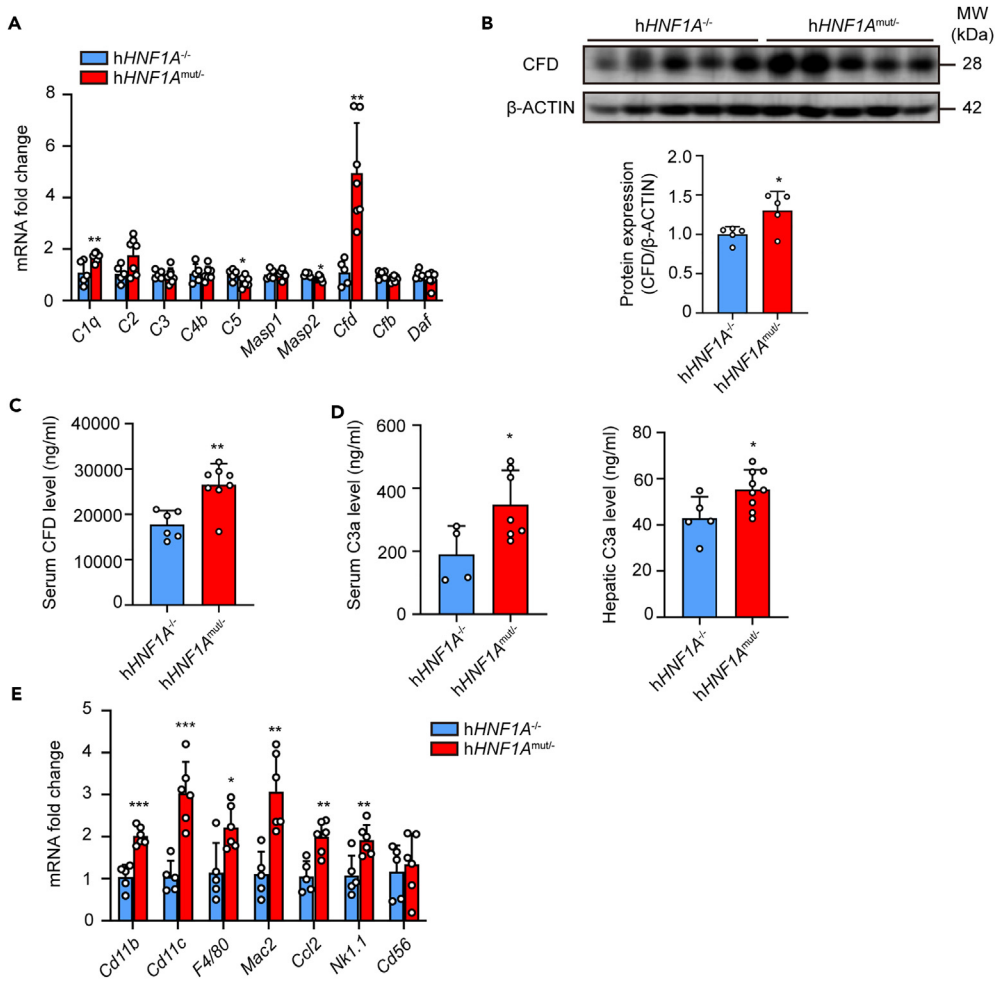

Figure 5. Complement factor D (CFD) and alternative complement pathway were stimulated in h*HNF1A*$^{mut/-}$ mice

(A) mRNA levels of genes relative to three complement pathways (n = 5 for h*HNF1A*$^{-/-}$ group, n = 7 for h*HNF1A*$^{mut/-}$ group).

(B) Protein levels of CFD and β-ACTIN in liver (n = 5 for each group).

(C and D) Concentration of serum CFD (C), serum and hepatic complement component 3a (C3a) (D) of 20-week-old male mice (n = 6 for h*HNF1A*$^{-/-}$ group, n = 8 for h*HNF1A*$^{mut/-}$ group for serum CFD levels, n = 4 for h*HNF1A*$^{-/-}$ group, n = 7 for h*HNF1A*$^{mut/-}$ group for serum C3a level, n = 5 for h*HNF1A*$^{-/-}$ group, n = 9 for h*HNF1A*$^{mut/-}$ group for hepatic C3a level).

(E) Hepatic immune infiltration of 20-week-old male mice was assessed by QPCR (n = 5 for h*HNF1A*$^{-/-}$ group, n = 6 for h*HNF1A*$^{mut/-}$ group). All data are presented as mean ± SD. *p < 0.05; **p < 0.01; ***p < 0.001 by an unpaired two-tailed t test. See also Figure S4.

generally diagnosed in adulthood after puberty, so whether there are abnormalities in liver lipid metabolism before the diagnosis of diabetes mellitus has not been widely investigated. Previous studies used to utilize knockout mice or β cell-specific human HNF1α mutant transgenic mice to study its effects on β cell function.[19] However, the age of onset and severity of disease are extremely heterogeneous in patients with MODY3.[38] Consequently, the establishment of an animal model with point mutation is of great importance to study the characteristics of patients and molecular changes. P291fsinsC is a high-frequency mutation in *HNF1A* used for *in vivo* and *in vitro* studies.[20,39] Besides, it has been observed that individuals with both MODY3 and liver adenomatosis have a much higher incidence of the P291fsinsC mutation than classical patients with MODY.[30] Based on these, this point mutation was chosen for constructing the global-expressed mutant mice in our study. We noticed that the dominant-negative mutant led to some developmental defects, such as reduced body length and weight. The *Hnf1a* knockout mice and *CMV* enhancer, porcine insulin promoter-driven *HNF1A* P291fsinsC transgenic models also exhibited the lower weight and growth retardation.[20,40] Changes in growth hormone levels and IGF-1 expression were previously reported in *Hnf1a* knockout mice, and although the mutant mice also suffer from growth retardation, we did not detect changes in serum levels of growth hormone and IGF-1. Considering that the cause of retarded growth is multifactorial and a recent study indicates that the truncated form of HNF1α expressed by P291fsinsC mutant might have additional HNF1α-independent functions by interacting with other HNF members, we speculate that the cause of developmental defects in h*HNF1A*$^{mut/-}$ mice may not be consistent with *Hnf1a* knockout mice and that the function of the truncated protein in different tissues and organs remains to be investigated in more depth.[41]

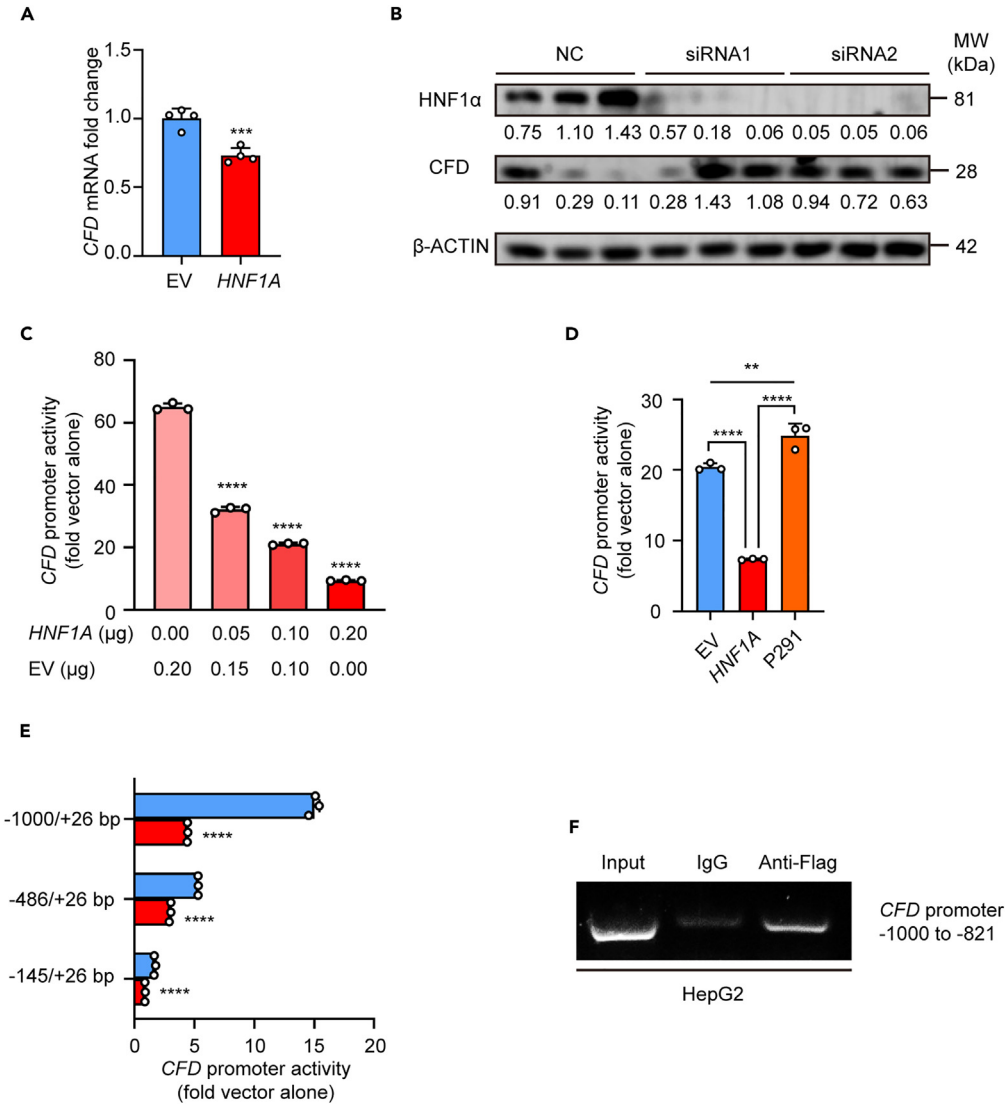

Figure 6. HNF1α negatively regulated the transcription of *CFD*

(A) mRNA level of *CFD* in HepG2 cells transfected with plasmids as indicated.

(B) Protein levels of HNF1α, CFD and β-ACTIN in AML12 cells after transfection with NC and siRNAs against mouse *Hnf1a*.

(C) Transcriptional activity of *CFD* promoter, transfected with increasing amounts of wild-type *HNF1A*.

(D) Transcriptional activity of *CFD* promoter, transfected with empty vector, wild-type and P291fsinsC mutant HNF1α.

(E) Transcriptional activities of *CFD* promoter with different lengths, transfected with empty vector or wild-type *HNF1A*.

(F) Chromatin immunoprecipitation (ChIP) assay result of HNF1α binding with *CFD* promoter from −1000bp to −821bp. The relative promoter luciferase activities were normalized by the activity of pRL-TK. The promoter activity was corrected by that obtained for the vector alone. EV: Empty Vector, *HNF1A*: *CMV-HNF1A*-Flag, P291: *CMV-HNF1A* P291fsinsC-Flag. All data were presented as mean ± SD. *p < 0.05; **p < 0.01; ****p < 0.0001 by Ordinary one-way ANOVA test. See also Figures S5–S7.

It is unexpected that the mice carrying a pathogenic MODY3 mutation did not develop early-onset diabetes, but only showed impaired insulin sensitivity during our observation. As we mentioned before, the characteristic of MODY3 is highly variable on the age of onset and symptom severity. Although the gene responsible for the disease is well defined, the mechanism and development of disease are complex. Besides, the worsening of GTT and ITT are associated with the long duration of pancreatic beta cell dysfunction and tissue insulin resistance. The single copy of mutant *HNF1A* expressed in our model might be contributed to the milder phenotype than what is observed in the patients with MODY3. Since h*HNF1A*$^{mut/-}$ mice were constructed via the ubiquitous expression of *Cag*-Cre, it is possible that the lack of a diabetic phenotype may be attributed to the complex interactions between multiple organs and tissues, as well as the relatively short observation period. In addition, the expression of the inserted human *HNF1A* mutant did not increase in pancreas, which could partially explain the absence of diabetic phenotype.

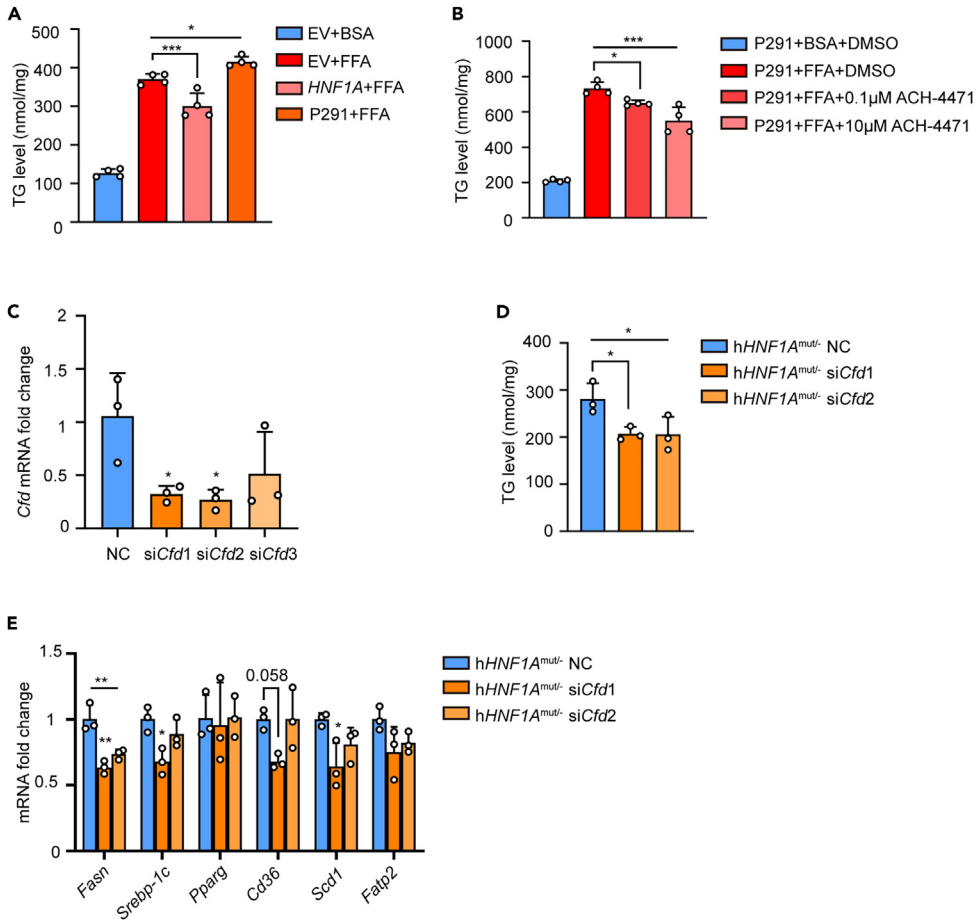

Figure 7. Overexpression of HNF1α or inhibition of CFD attenuated triglyceride accumulation in free fatty acid (FFA) induced HepG2 cells and primary hepatocytes of h*HNF1A*$^{mut/-}$ mice

(A and B) The TG content in FFA-pretreated HepG2 cells transfected with WT HNF1α and HNF1α P291fsinsC mutation (A) or treated with CFD inhibitor ACH-4471 (B).

(C) The knockdown efficiency of three mouse *Cfd* siRNAs.

(D and E) The TG level (D) and the expression of genes related to *de novo* lipogenesis (*Fasn*, *Srebp-1c*, *Scd1*) and fatty acid uptake (*Pparg*, *Cd36* and *Fatp2*) (E) of the primary hepatocytes of h*HNF1A*$^{mut/-}$ mice transfected with si*Cfd*1 and si*Cfd*2. All data were presented as mean ± SD. *p < 0.05; **p < 0.01; ***p < 0.001 by Ordinary one-way ANOVA test.

Several studies have reported that patients with MODY3 may develop hepatocellular adenoma or liver adenomatosis.[30,42] These adenomas are typically characterized by macrovesicular and microvesicular steatosis.[35] It is reported that the liver dysfunction and steatosis occurred in the early childhood of a Japanese girl, before she was diagnosed as MODY3.[43] At that time, her HbA1c and blood glucose levels were both within normal range. A French series of patients with MODY3 with liver adenomatosis also showed that the glucose control didn't affect the development of adenoma.[30] In addition, Joan-Marc Servitja et al. and Duncan T. Odom et al. found that *HNF1A* controlled highly tissue-specific regulatory networks in the liver and pancreas.[6,44] These findings indicated that the disorders of lipid metabolism in liver caused by the P291fsinsC mutation or other *HNF1A* mutations may not be a consequence of impaired glucose regulation.

Previous studies have reported the significant involvement of HNF1α in the hepatic lipid metabolism.[13,14] However, the RNA-seq results of human liver samples with *HNF1A* biallelic mutation have revealed that the promotion of lipogenesis in the insufficiency is independent of SREBP-1C and carbohydrate-response element-binding protein (CHREBP).[11] The expression of SREBP-1C is not significantly changed between h*HNF1A*$^{mut/-}$ and h*HNF1A*$^{-/-}$group, which is consistent with this finding. On the other hand, despite the dramatic increase in FASN expression in the liver of h*HNF1A*$^{mut/-}$ mice, it is thought that the increase in FASN is a subsequent event, as a previous study have demonstrated that FASN is not directly regulated by HNF1α.[45] We observed a significant elevation in *Pparg* mRNA levels within the livers of h*HNF1A*$^{mut/-}$ mice. However, in terms of PPARγ protein expression, there was no statistical significance between the h*HNF1A*$^{mut/-}$ and h*HNF1A*$^{-/-}$ groups, despite a slight trend of increased expression. Previous studies that suggest a role for HNF1α in inhibiting *PPARG* transcription during hepatocellular carcinoma (HCC) development.[13] Therefore, we proceeded to examine the expression of PPARγ target genes

in the liver. As depicted in Figure S8, the expressions of Phosphoenolpyruvate carboxykinase 1 (*Pck1*), phosphoenolpyruvate carboxykinase 2 (*Pck2*), and fatty acid binding protein 4 (*Fabp4*) did not exhibit significant differences. The mRNA level of lipoprotein lipase (*Lpl*) was notably elevated by approximately 3-fold in the livers of the h*HNF1A*$^{mut/-}$ group compared to the h*HNF1A*$^{-/-}$ group. While we cannot entirely dismiss the possibility of PPARγ playing a role in hepatic lipid accumulation in mutant mice, the molecular mechanism underlying *HNF1A* deficiency-induced liver lipid deposition requires further investigation.

According to the transcriptome and proteome analysis, upregulated genes were mainly involved in inflammation and lipid metabolic processes. We wondered if there were intermediary agents that upregulated by dominant negative HNF1α mutant, promoting the lipid accumulation and inflammation in the liver. Interestingly, the transcriptional level of *Cfd*, which is typically expressed at high levels in adipose tissues rather than liver, was dramatically upregulated in h*HNF1A*$^{mut/-}$ liver. The knockout of *Cfd* in liver could effectively reduce the liver steatosis and inflammatory infiltration.[27] Furthermore, CFD serves as the primary catalyst for the activation of C3 in the alternative complement pathway, leading to the production of C3a.[34] C3a undergoes rapid cleavage by carboxypeptidase B or carboxypeptidase N, resulting in the formation of C3adesArg, also known as acylation-stimulating protein (ASP).[46] It is reported that ASP, which constitutes the predominant form of circulating C3a, can substantially stimulate the TG synthesis and glucose transport in adipose tissue.[47,48] Besides, the C3a and ASP are closely related to the development of NAFLD and hepatic inflammation.[25,49] In agreement with these studies, the concentrations of serum CFD and its direct cleavage product C3a increased in h*HNF1A*$^{mut/-}$ mice. The results suggested that the hepatic steatosis and inflammation in the liver could be, at least partially explained by the abnormal production and secretion of CFD.

HNF1A regulates the expression of certain components of the classical complement pathway, such as C5 and C8a.[28] In the liver of h*HNF1A*$^{mut/-}$ mice, the expression of C5 was found to be downregulated. However, it is not known yet whether CFD is regulated by HNF1α. For the first time, we found that the transcription of *CFD* was negatively regulated by HNF1α. According to the luciferase assay, HNF1α could inhibit the transcription activity of *CFD* promoter, despite the fact that the promoter was a mere 200 base pairs in length, located proximal to the transcription start site. ChIP assay suggested a potential binding region for HNF1α within the sequence spanning from −1000bp to −821bp of the *CFD* promoter. However, the classical HNF1α binding motif (5′-GTTAATNATTAAC-3′) was not identified within the approximately 1000bp promoter sequence. Given that HNF1α engages with a multitude of binding partners,[50] it is conceivable that HNF1α might exert its inhibitory effect on *CFD* expression through its interaction with these partners. Further investigations are imperative to unveil the underlying mechanism by which HNF1α modulates the transcriptional regulation of the *CFD* gene. In addition, CFD is an adipokine and a constituent of the alternative complement pathway, it is synthesized and secreted into the bloodstream, where it exerts its effects. However, it is unclear whether the ectopic expression of CFD affected directly on hepatocytes or other cell types within liver. Nonetheless, we found that selective small-molecule inhibitor against CFD could suppress the triglyceride accumulation in FFA-pretreated HepG2 cells, which indicated CFD might directly regulate triglyceride synthesis in the hepatocyte *in vitro*. The conditional *Cfd* knockout mice might be used for revealing the intricate regulation of CFD and its impact on the progression of NAFLD.

In conclusion, our findings demonstrate that h*HNF1A*$^{mut/-}$ mice displayed spontaneous hepatic steatosis and inflammation, and the suppression of CFD may be one of the potential mechanisms responsible for delaying NAFLD progression. Patients with MODY3 should be vigilant about their liver function, and regular follow-ups should be conducted.

Limitations of the study

In our study, the human *HNF1A* CDS with P291fsinsC mutation was inserted and induced by the globally expressed *Cag*-Cre, resulting in the augmented expression of the exogenous HNF1α mutant. However, this extensive overexpression of the mutant exhibited certain undesirable outcomes, including growth retardation and developmental anomalies, which do not accurately mirror the physiological conditions of human HNF1α P291fsinsC carriers. Furthermore, our study focused on a single gender of mice, limiting the comprehensive understanding of the liver's pathological processes and gender-specific differences. Additionally, there exists a dearth of conclusive evidence elucidating the role of CFD in promoting liver steatosis and inflammation, achieved through specific knockout of *Cfd* within the liver of h*HNF1A*$^{mut/-}$ mice. The intricate mechanism underlying CFD-mediated promotion of hepatic lipogenesis warrants further rigorous investigation.

STAR★METHODS

Detailed methods are provided in the online version of this paper and include the following:

- KEY RESOURCES TABLE
- RESOURCE AVAILABILITY
  - Lead contact
  - Materials availability
  - Data and code availability
- EXPERIMENTAL MODEL AND STUDY PARTICIPANT DETAILS
  - Animals
  - Cell lines and primary cultures
- METHOD DETAILS
  - Metabolic parameters and studies
  - Histology

- Western blotting
- Quantitative real-time PCR
- Transcriptome analysis
- Proteome analysis
- Transient transfection and FFA incubation
- Luciferase reporter assay
- Chromatin immunoprecipitation (ChIP) assay
- Primary hepatocyte isolation
- Gene correlation analysis

● QUANTIFICATION AND STATISTICAL ANALYSIS

SUPPLEMENTAL INFORMATION

Supplemental information can be found online at https://doi.org/10.1016/j.isci.2023.108018.

ACKNOWLEDGMENTS

This work was supported by grants from the National Natural Science Foundation of China (Grant NO. 91957209, 82130025, 82200947 and 82200659), and the Natural Science Foundation of Shandong Province (Grant NO. ZR2022QH002). We thank the Model Animal Research Institute and central laboratory of Shandong Provincial Hospital for providing animal management services and instrument platform support for our work. The graphical abstract was made by Figdraw.

AUTHOR CONTRIBUTIONS

Conceptualization and supervision, P.L., J.Z., and S.S.; investigation and validation, M.L.; formal analysis, M.L., L.L., H.G., and X.F.; visualization, M.L.; writing - original draft, P.L and M.L.; writing - review & editing, Y.S., L.G., Z.H., C.X., T.L., P.L., J.Z., and S.S.

DECLARATION OF INTERESTS

The authors declare no competing interests.

INCLUSION AND DIVERSITY

We support inclusive, diverse, and equitable conduct of research.

Received: May 18, 2023
Revised: August 14, 2023
Accepted: September 19, 2023
Published: September 22, 2023

REFERENCES

1. Friedman, S.L., Neuschwander-Tetri, B.A., Rinella, M., and Sanyal, A.J. (2018). Mechanisms of NAFLD development and therapeutic strategies. Nat. Med. *24*, 908–922. https://doi.org/10.1038/s41591-018-0104-9.
2. Juanola, O., Martínez-López, S., Francés, R., and Gómez-Hurtado, I. (2021). Non-Alcoholic Fatty Liver Disease: Metabolic, Genetic, Epigenetic and Environmental Risk Factors. Int. J. Environ. Res. Public Health *18*, 5227. https://doi.org/10.3390/ijerph18105227.
3. Ahadi, M., Molooghi, K., Masoudifar, N., Namdar, A.B., Vossoughinia, H., and Farzanehfar, M. (2021). A review of non-alcoholic fatty liver disease in non-obese and lean individuals. J. Gastroenterol. Hepatol. *36*, 1497–1507. https://doi.org/10.1111/jgh.15353.
4. Miyachi, Y., Miyazawa, T., and Ogawa, Y. (2022). HNF1A Mutations and Beta Cell Dysfunction in Diabetes. Int. J. Mol. Sci. *23*, 3222. https://doi.org/10.3390/ijms23063222.
5. Valkovicova, T., Skopkova, M., Stanik, J., and Gasperikova, D. (2019). Novel insights into genetics and clinics of the HNF1A-MODY. Endocr. Regul. *53*, 110–134. https://doi.org/10.2478/enr-2019-0013.
6. Servitja, J.M., Pignatelli, M., Maestro, M.A., Cardalda, C., Boj, S.F., Lozano, J., Blanco, E., Lafuente, A., McCarthy, M.I., Sumoy, L., et al. (2009). Hnf1alpha (MODY3) controls tissue-specific transcriptional programs and exerts opposed effects on cell growth in pancreatic islets and liver. Mol. Cell Biol. *29*, 2945–2959. https://doi.org/10.1128/MCB.01389-08.
7. Beaufrère, A., and Paradis, V. (2021). Hepatocellular adenomas: review of pathological and molecular features. Hum. Pathol. *112*, 128–137. https://doi.org/10.1016/j.humpath.2020.11.016.
8. Bioulac-Sage, P., Sempoux, C., and Balabaud, C. (2017). Hepatocellular adenoma: Classification, variants and clinical relevance. Semin. Diagn. Pathol. *34*, 112–125. https://doi.org/10.1053/j.semdp.2016.12.007.
9. Behl, R., Malhotra, N., Joshi, V., Poojary, S., Middha, S., Gupta, S., Olaonipekun, A.B., Okoye, I., Wagh, B., Biswas, D., et al. (2022). Meta-analysis of HNF1A-MODY3 variants among human population. J. Diabetes Metab. Disord. *21*, 1037–1046. https://doi.org/10.1007/s40200-022-00975-8.
10. Lee, Y.H., Sauer, B., and Gonzalez, F.J. (1998). Laron dwarfism and non-insulin-dependent diabetes mellitus in the Hnf-1alpha knockout mouse. Mol. Cell Biol. *18*, 3059–3068. https://doi.org/10.1128/mcb.18.5.3059.
11. Liu, F., Zhu, X., Jiang, X., Li, S., and Lv, Y. (2022). Transcriptional control by HNF-1: Emerging evidence showing its role in lipid metabolism and lipid metabolism disorders. Genes Dis. *9*, 1248–1257. https://doi.org/10.1016/j.gendis.2021.06.010.
12. Qin, Y., Qiu, D., and Zhang, Q. (2023). HNF1A regulates the crosstalk between innate immune responses and MAFLD by mediating autophagic degradation of TBK1. Autophagy *19*, 1026–1027. https://doi.org/10.1080/15548627.2022.2110728.
13. Patitucci, C., Couchy, G., Bagattin, A., Cañeque, T., de Reyniès, A., Scoazec, J.Y., Rodriguez, R., Pontoglio, M., Zucman-Rossi, J., Pende, M., and Panasyuk, G. (2017).

Hepatocyte nuclear factor 1α suppresses steatosis-associated liver cancer by inhibiting PPARγ transcription. J. Clin. Invest. *127*, 1873–1888. https://doi.org/10.1172/jci90327.

14. Tan, J., Xu, J., Wei, G., Zhang, L., Sun, L., Wang, G., Li, F., and Jiang, F. (2019). HNF1α Controls Liver Lipid Metabolism and Insulin Resistance via Negatively Regulating the SOCS-3-STAT3 Signaling Pathway. J. Diabetes Res. *2019*, 5483946. https://doi.org/10.1155/2019/5483946.
15. Hu, M., Huang, X., Han, X., and Ji, L. (2020). Loss of HNF1α Function Contributes to Hepatocyte Proliferation and Abnormal Cholesterol Metabolism via Downregulating miR-122: A Novel Mechanism of MODY3. Diabetes Metab. Syndr. Obes. *13*, 627–639. https://doi.org/10.2147/dmso.S236915.
16. Kakuda, K., Niwa, A., Honda, R., Yamaguchi, K.I., Tomita, H., Nojebuzzaman, M., Hara, A., Goto, Y., Osawa, M., and Kuwata, K. (2019). A DISC1 point mutation promotes oligomerization and impairs information processing in a mouse model of schizophrenia. J. Biochem. *165*, 369–378. https://doi.org/10.1093/jb/mvy116.
17. Powell, D.A., Hsu, A.P., Shubitz, L.F., Butkiewicz, C.D., Moale, H., Trinh, H.T., Doetschman, T., Georgieva, T.G., Reinartz, D.M., Wilson, J.E., et al. (2022). Mouse Model of a Human STAT4 Point Mutation That Predisposes to Disseminated Coccidiomycosis. Immunohorizons *6*, 130–143. https://doi.org/10.4049/immunohorizons.2200007.
18. Testa, G., Mainardi, M., Morelli, C., Olimpico, F., Pancrazi, L., Petrella, C., Severini, C., Florio, R., Malerba, F., Stefanov, A., et al. (2019). The NGF(R100W) Mutation Specifically Impairs Nociception without Affecting Cognitive Performance in a Mouse Model of Hereditary Sensory and Autonomic Neuropathy Type V. J. Neurosci. *39*, 9702–9715. https://doi.org/10.1523/jneurosci.0688-19.2019.
19. Li, L.M., Jiang, B.G., and Sun, L.L. (2022). HNF1A:From Monogenic Diabetes to Type 2 Diabetes and Gestational Diabetes Mellitus. Front. Endocrinol. *13*, 829565. https://doi.org/10.3389/fendo.2022.829565.
20. Umeyama, K., Nakajima, M., Yokoo, T., Nagaya, M., and Nagashima, H. (2017). Diabetic phenotype of transgenic pigs introduced by dominant-negative mutant hepatocyte nuclear factor 1alpha. J. Diabetes Complications *31*, 796–803. https://doi.org/10.1016/j.jdiacomp.2017.01.025.
21. Mikkelsen, R.B., Arora, T., Trošt, K., Dmytriyeva, O., Jensen, S.K., Meijnikman, A.S., Olofsson, L.E., Lappa, D., Aydin, Ö., Nielsen, J., et al. (2022). Type 2 diabetes is associated with increased circulating levels of 3-hydroxydecanoate activating GPR84 and neutrophil migration. iScience *25*, 105683. https://doi.org/10.1016/j.isci.2022.105683.
22. Coss, S.L., Zhou, D., Chua, G.T., Aziz, R.A., Hoffman, R.P., Wu, Y.L., Ardoin, S.P., Atkinson, J.P., and Yu, C.Y. (2023). The complement system and human autoimmune diseases. J. Autoimmun. *137*, 102979. https://doi.org/10.1016/j.jaut.2022.102979.
23. Thorgersen, E.B., Barratt-Due, A., Haugaa, H., Harboe, M., Pischke, S.E., Nilsson, P.H., and Mollnes, T.E. (2019). The Role of Complement in Liver Injury, Regeneration, and Transplantation. Hepatology *70*, 725–736. https://doi.org/10.1002/hep.30508.
24. Trouw, L.A., Pickering, M.C., and Blom, A.M. (2017). The complement system as a potential therapeutic target in rheumatic disease. Nat. Rev. Rheumatol. *13*, 538–547. https://doi.org/10.1038/nrrheum.2017.125.
25. Zhao, J., Wu, Y., Lu, P., Wu, X., Han, J., Shi, Y., Liu, Y., Cheng, Y., Gao, L., Zhao, J., et al. (2022). Association of complement components with the risk and severity of NAFLD: A systematic review and meta-analysis. Front. Immunol. *13*, 1054159. https://doi.org/10.3389/fimmu.2022.1054159.
26. Han, J., and Zhang, X. (2021). Complement Component C3: A Novel Biomarker Participating in the Pathogenesis of Non-alcoholic Fatty Liver Disease. Front. Med. *8*, 653293. https://doi.org/10.3389/fmed.2021.653293.
27. Tsuru, H., Osaka, M., Hiraoka, Y., and Yoshida, M. (2020). HFD-induced hepatic lipid accumulation and inflammation are decreased in Factor D deficient mouse. Sci. Rep. *10*, 17593. https://doi.org/10.1038/s41598-020-74617-5.
28. Peixoto-Barbosa, R., Reis, A.F., and Giuffrida, F.M.A. (2020). Update on clinical screening of maturity-onset diabetes of the young (MODY). Diabetol. Metab. Syndr. *12*, 50. https://doi.org/10.1186/s13098-020-00557-9.
29. Fred, R.G., Steen Pedersen, J., Thompson, J.J., Lee, J., Timshel, P.N., Stender, S., Opseth Rygg, M., Gluud, L.L., Bjerregaard Kristiansen, V., Bendtsen, F., et al. (2022). Single-cell transcriptome and cell type-specific molecular pathways of human non-alcoholic steatohepatitis. Sci. Rep. *12*, 13484. https://doi.org/10.1038/s41598-022-16754-7.
30. Haddouche, A., Bellanne-Chantelot, C., Rod, A., Fournier, L., Chiche, L., Gautier, J.F., Timsit, J., Laboureau, S., Chaillous, L., Valero, R., et al. (2020). Liver adenomatosis in patients with hepatocyte nuclear factor-1 alpha maturity onset diabetes of the young (HNF1A-MODY): Clinical, radiological and pathological characteristics in a French series. J. Diabetes *12*, 48–57. https://doi.org/10.1111/1753-0407.12959.
31. Yamagata, K., Oda, N., Kaisaki, P.J., Menzel, S., Furuta, H., Vaxillaire, M., Southam, L., Cox, R.D., Lathrop, G.M., Boriraj, V.V., et al. (1996). Mutations in the hepatocyte nuclear factor-1alpha gene in maturity-onset diabetes of the young (MODY3). Nature *384*, 455–458. https://doi.org/10.1038/384455a0.
32. Kaisaki, P.J., Menzel, S., Lindner, T., Oda, N., Rjasanowski, I., Sahm, J., Meincke, G., Schulze, J., Schmechel, H., Petzold, C., et al. (1997). Mutations in the hepatocyte nuclear factor-1alpha gene in MODY and early-onset NIDDM: evidence for a mutational hotspot in exon 4. Diabetes *46*, 528–535. https://doi.org/10.2337/diab.46.3.528.
33. Ni, Q., Ding, K., Wang, K.Q., He, J., Yin, C., Shi, J., Zhang, X., Xie, W.F., and Shi, Y.Q. (2017). Deletion of HNF1alpha in hepatocytes results in fatty liver-related hepatocellular carcinoma in mice. FEBS Lett. *591*, 1947–1957. https://doi.org/10.1002/1873-3468.12689.
34. Barratt, J., and Weitz, I. (2021). Complement Factor D as a Strategic Target for Regulating the Alternative Complement Pathway. Front. Immunol. *12*, 712572. https://doi.org/10.3389/fimmu.2021.712572.
35. Bioulac-Sage, P., Sempoux, C., and Balabaud, C. (2017). Hepatocellular Adenomas: Morphology and Genomics. Gastroenterol. Clin. North Am. *46*, 253–272. https://doi.org/10.1016/j.gtc.2017.01.003.
36. Li, X.J., Shao, D.H., He, M.L., and Liang, G.W. (2019). Association of Common Variants in HNF1A Gene with Serum AFP Level in Healthy Chinese Individuals and HCC Patients. Dis. Markers *2019*, 6273497. https://doi.org/10.1155/2019/6273497.
37. Shah, P., Rahman, S.A., Demirbilek, H., Güemes, M., and Hussain, K. (2017). Hyperinsulinaemic hypoglycaemia in children and adults. Lancet Diabetes Endocrinol. *5*, 729–742. https://doi.org/10.1016/s2213-8587(16)30323-0.
38. Hermann, F.M., Kjærgaard, M.F., Tian, C., Tiemann, U., Jackson, A., Olsen, L.R., Kraft, M., Carlsson, P.O., Elfving, I.M., Kettunen, J.L.T., et al. (2023). An insulin hypersecretion phenotype precedes pancreatic β cell failure in MODY3 patient-specific cells. Cell Stem Cell *30*, 38–51.e8. https://doi.org/10.1016/j.stem.2022.12.001.
39. Adams, M.T., and Blum, B. (2022). Determinants and dynamics of pancreatic islet architecture. Islets *14*, 82–100. https://doi.org/10.1080/19382014.2022.2030649.
40. Sato, Y., Rahman, M.M., Haneda, M., Tsuyama, T., Mizumoto, T., Yoshizawa, T., Kitamura, T., Gonzalez, F.J., Yamamura, K.I., and Yamagata, K. (2020). HNF1α controls glucagon secretion in pancreatic α-cells through modulation of SGLT1. Biochim. Biophys. Acta, Mol. Basis Dis. *1866*, 165898. https://doi.org/10.1016/j.bbadis.2020.165898.
41. Cujba, A.M., Alvarez-Fallas, M.E., Pedraza-Arevalo, S., Laddach, A., Shepherd, M.H., Hattersley, A.T., Watt, F.M., and Sancho, R. (2022). An HNF1α truncation associated with maturity-onset diabetes of the young impairs pancreatic progenitor differentiation by antagonizing HNF1β function. Cell Rep. *38*, 110425. https://doi.org/10.1016/j.celrep.2022.110425.
42. Nault, J.C., Paradis, V., Ronot, M., and Zucman-Rossi, J. (2022). Benign liver tumours: understanding molecular physiology to adapt clinical management. Nat. Rev. Gastroenterol. Hepatol. *19*, 703–716. https://doi.org/10.1038/s41575-022-00643-5.
43. Nakamura, A., Ishidu, K., and Tajima, T. (2012). Early onset of liver steatosis in a Japanese girl with maturity-onset diabetes of the young type 3 (MODY3). J. Clin. Res. Pediatr. Endocrinol. *4*, 104–106. https://doi.org/10.4274/jcrpe.584.
44. Odom, D.T., Zizlsperger, N., Gordon, D.B., Bell, G.W., Rinaldi, N.J., Murray, H.L., Volkert, T.L., Schreiber, J., Rolfe, P.A., Gifford, D.K., et al. (2004). Control of pancreas and liver gene expression by HNF transcription factors. Science *303*, 1378–1381. https://doi.org/10.1126/science.1089769.
45. Pelletier, L., Rebouissou, S., Paris, A., Rathahao-Paris, E., Perdu, E., Bioulac-Sage, P., Imbeaud, S., and Zucman-Rossi, J. (2010). Loss of hepatocyte nuclear factor 1α function in human hepatocellular adenomas leads to aberrant activation of signaling pathways involved in tumorigenesis. Hepatology *51*, 557–566. https://doi.org/10.1002/hep.23362.
46. Sathyapalan, T., Hobkirk, J.P., Javed, Z., Carroll, S., Coady, A.M., Pemberton, P., Smith, A., Cianflone, K., and Atkin, S.L. (2019). The Effect of Atorvastatin (and Subsequent Metformin) on Adipose Tissue Acylation-Stimulatory-Protein Concentration and Inflammatory Biomarkers in Overweight/Obese Women With Polycystic Ovary Syndrome. Front. Endocrinol. *10*, 394. https://doi.org/10.3389/fendo.2019.00394.

47. Ochiai, M. (2020). Evaluating the appropriate oral lipid tolerance test model for investigating plasma triglyceride elevation in mice. PLoS One *15*, e0235875. https://doi.org/10.1371/journal.pone.0235875.

48. Vlaicu, S.I., Tatomir, A., Boodhoo, D., Vesa, S., Mircea, P.A., and Rus, H. (2016). The role of complement system in adipose tissue-related inflammation. Immunol. Res. *64*, 653–664. https://doi.org/10.1007/s12026-015-8783-5.

49. Guo, Z., Fan, X., Yao, J., Tomlinson, S., Yuan, G., and He, S. (2022). The role of complement in nonalcoholic fatty liver disease. Front. Immunol. *13*, 1017467. https://doi.org/10.3389/fimmu.2022.1017467.

50. Yu, M., Wang, J., Li, W., Yuan, Y.Z., Li, C.Y., Qian, X.H., Xu, W.X., Zhan, Y.Q., and Yang, X.M. (2008). Proteomic screen defines the hepatocyte nuclear factor 1alpha-binding partners and identifies HMGB1 as a new cofactor of HNF1alpha. Nucleic Acids Res. *36*, 1209–1219. https://doi.org/10.1093/nar/gkm1131.

51. Zhou, Y., Zhou, B., Pache, L., Chang, M., Khodabakhshi, A.H., Tanaseichuk, O., Benner, C., and Chanda, S.K. (2019). Metascape provides a biologist-oriented resource for the analysis of systems-level datasets. Nat. Commun. *10*, 1523. https://doi.org/10.1038/s41467-019-09234-6.

52. Tian, L., Song, Y., Xing, M., Zhang, W., Ning, G., Li, X., Yu, C., Qin, C., Liu, J., Tian, X., et al. (2010). A novel role for thyroid-stimulating hormone: up-regulation of hepatic 3-hydroxy-3-methyl-glutaryl-coenzyme A reductase expression through the cyclic adenosine monophosphate/protein kinase A/cyclic adenosine monophosphate-responsive element binding protein pathway. Hepatology *52*, 1401–1409. https://doi.org/10.1002/hep.23800.

STAR★METHODS

KEY RESOURCES TABLE

REAGENT or RESOURCE	SOURCE	IDENTIFIER
Antibodies		
Rabbit monoclonal anti-FASN (Western blot 1:1000)	Cell Signaling Technology, USA	Cat#3180; RRID: AB_2100796
Mouse monoclonal anti-SREBP-1C (Western blot 1:1000)	Novus, USA	Cat#NB600-582; RRID: AB_10001575
Rabbit polyclonal anti-CD36 (Western blot 1:1000)	Proteintech Co Ltd, USA	Cat#18836; RRID: AB_10597244
Rabbit monoclonal anti-PPARγ (Western blot 1:1000)	Cell Signaling Technology, USA	Cat#2443; RRID: AB_823598
Mouse monoclonal anti-SCD1 (Western blot 1:1000)	Abcam, USA	Cat#ab19862; RRID: AB_445179
Mouse monoclonal anti-CFD (Western blot 1:100)	Santa Cruz Biotechnology, USA	Cat#sc376015; RRID: AB_11008481
Mouse monoclonal anti-β-ACTIN (Western blot 1:7500)	Proteintech Co Ltd, USA	Cat#66009-1-Ig; RRID: AB_2687938
Rabbit monoclonal anti-HNF1A (Western blot 1:1000 IHC 1:200)	Cell Signaling Technology, USA	Cat#89670; RRID: AB_2728751
Normal mouse IgG	Santa Cruz Biotechnology, USA	Cat#sc3877; RRID: AB_737222
Mouse monoclonal Anti-Flag	Sigma, USA	Cat#F1804; RRID: AB_262044
Bacterial and virus strains		
pAAV-TBG-sfEGFP-3Flag-mir30shRNA (*Hnf1a*)-WPRE	This paper, OBiO Technology (Shanghai, China)	N/A
pAAV-TBG-sfEGFP-3Flag-mir30shRNA (NC)-WPRE	This paper, OBiO Technology (Shanghai, China)	N/A
Chemicals, peptides, and recombinant proteins		
ACH-4471	Selleck, USA	Cat#S0803
TRIzol reagent	Vazyme, (Nanjing, China)	Cat#R401-01
Phosphatase inhibitor cocktail	Bimake, USA	Cat#B15001
Oleic acid	Sigma, USA	Cat#O1008
Palmitic acid	Sigma, USA	Cat#P5585
Critical commercial assays		
Mouse Growth Hormone ELISA kit	CUSABIO (Wuhan, China)	Cat# CSB-E07343m
Mouse Insulin-Like Growth Factor 1 (IGF-1) ELISA kit	CUSABIO (Wuhan, China)	Cat# CSB-E04581m
Mouse Complement Factor D ELISA kit	MULTISCIENCES, (Hangzhou, China)	Cat#EK-1290
Mouse Complement 3a (C3a) ELISA kit	CLOUD-CLONE CORP (Wuhan, China)	Cat#SEA387Mu
Tissue or Cell Triglyceride test kit	APPLYGEN (Beijing, China)	Cat#E1013
Tissue or Cell Total Cholesterol test kit	APPLYGEN (Beijing, China)	Cat#E1015
Tissue Free Cholesterol test kit	APPLYGEN (Beijing, China)	Cat#E1016
Dual-Luciferase® Reporter Assay System	Promega, USA	Cat#E1910
Lipofectamine® 3000 Transfection Kit	Invitrogen, USA	Cat#L3000015
QuickMutation™ Site-Directed Mutagenesis Kit	Beyotime, China	Cat#D0206

(*Continued on next page*)

Continued

REAGENT or RESOURCE	SOURCE	IDENTIFIER
Hifair®III 1st Strand cDNA Synthesis	Yeasen Biotechnology (Shanghai, China)	Cat#11141ES60
SYBR Green	Yeasen Biotechnology (Shanghai, China)	Cat#11201ES03
Deposited data		
RNA-seq	This paper	GEO: GSE224953
Proteomic	This paper	iProX: PXD040561
Western blot original data	This paper Science Data Bank	Science data bank: https://www.scidb.cn/s/M7VNN3
Experimental models: Cell lines		
HepG2 cells	National Collection of Authenticated Cell Cultures, China	SCSP-510
AML12 cells	National Collection of Authenticated Cell Cultures, China	GNM42
293T cells	National Collection of Authenticated Cell Cultures, China	SCSP-502
Experimental models: Organisms/strains		
Mouse: h*HNF1A*$^{mut/-}$ mice: *HNF1A* KI/+; *Cag* Cre+	This paper, GemPharmatech (Nanjing, China)	N/A
Mouse: h*HNF1A*$^{-/-}$ mice: *HNF1A* KI/+; *Cag* Cre-	This paper, GemPharmatech (Nanjing, China)	N/A
Oligonucleotides		
Human *HNF1A* CDS primers Forward: 5′-atggtttctaaactgagccagctgc-3′	This paper	N/A
Human *HNF1A* CDS primers Reverse: 5′-ttactgggaggaagaggccatct-3′	This paper	N/A
Hnf1a siRNA1 5′-gaagatggtcaagtcgtactt-3′	This paper, Tsingke Biotech (Beijing, China)	N/A
Hnf1a siRNA2 5′-gtatcagagttccgactccaa-3′	This paper, Tsingke Biotech (Beijing, China)	N/A
Cfd siRNA1 5′-gcatcaactcagagtgtca-3′	This paper, Tsingke Biotech (Beijing, China)	N/A
Cfd siRNA2 5′-cgtctatacccgagtgtca-3′	This paper, Tsingke Biotech (Beijing, China)	N/A
Cfd siRNA3 5′-cttgcaatacgaggacaaa-3′	This paper, Tsingke Biotech (Beijing, China)	N/A
ChIP primers Forward: 5′-taatttttttgtagagatggggtctcgc-3′	This paper	N/A
ChIP primers Reverse: 5′-ccctcccaaactgttcactgag-3′	This paper	N/A
qRT-PCR primers, see Table S2	This paper	N/A
Recombinant DNA		
Plasmid: *CMV-HNF1A*-Flag	This paper	N/A
Plasmid: *CMV-HNF1A* P291fsinsC-Flag	This paper	N/A
Plasmid: pGL4.14-*CFD* promoter (-1000/+26bp)	This paper, Xitubio Biotechnology (Shanghai, China)	N/A
Plasmid: pGL4.14-*CFD* promoter (-486/+26bp)	This paper, Xitubio Biotechnology (Shanghai, China)	N/A

(*Continued on next page*)

Continued

REAGENT or RESOURCE	SOURCE	IDENTIFIER
Plasmid: pGL4.14-*CFD* promoter (-145/+26bp)	This paper, Xitubio Biotechnology (Shanghai, China)	N/A
Software and algorithms		
Image J	NIH, USA	N/A
SPSS 26.0 software	IBM, USA	N/A
GraphPad Prism 8	GraphPad Software, USA	N/A
TissueFAXS Viewer 7.1	TG (Beijing, China)	N/A

RESOURCE AVAILABILITY

Lead contact

Further information and requests for data and resources should be directed to and will be fulfilled by the Lead Contact, Peng Lu (sibslp@126.com).

Materials availability

All unique reagents generated in this study are available from the lead contact upon request.

Data and code availability

- RNA-seq data have been deposited at GEO, Proteomic data have been deposited at iProX and they are publicly available. Accession numbers are listed in the key resources table. Original western blot images have been deposited at Science data bank and are publicly available. The DOI is listed in the key resources table.
- This paper does not report original code.
- Any additional information required to reanalyze the data reported in this paper is available from the lead contact upon request.

EXPERIMENTAL MODEL AND STUDY PARTICIPANT DETAILS

Animals

A targeting vector containing *CAG*-LSL-*HNF1A* (with P291fsinsC mutation)-polyA segment (GenBank: NM_001306179) was inserted into H11 site of C57/B6J mice to generate h*HNF1A* flox mice (GemPharmatech). During the breeding process, male h*HNF1A*$^{fl/fl}$ mice were mated with female *Cag* Cre mice to produce the heterozygous h*HNF1A*$^{mut/-}$mice, and their littermates h*HNF1A*$^{-/-}$ were used as control mice. The AAV-*TBG*-shRNA (NC) and AAV-*TBG*-shRNA (*Hnf1a*) particles were provided by OBiO Technology. 7X10^{11} adenovirus particles were administrated to 8-week-old WT male mice by tail vein. The mice were sacrificed after 10 weeks of high-fat-diet feeding. The mice were maintained under specific pathogen-free conditions in a 12-h light/12-h dark cycle with unrestricted access to water and normal chow. Room temperature was maintained at 22±2°C. All the procedures were approved by the ethics committee of the Shandong Provincial Hospital (NO.2018-018).

Cell lines and primary cultures

HepG2, AML12 and 293T cells were purchased from National Collection of Authenticated Cell Cultures. Cells were utilized between passage 5-25. HepG2 cells were cultured in Minimum Essential Medium (GIBCO, 41500034), NaHCO3 1.5g/L, Sodium Pyruvate 0.11g/L. AML12 cells were cultured in Dulbecco's Modified Eagle Medium/Nutrient Mixture F-12 (GIBCO, C11330500BT), Dexamethasone 40 ng/ml, ITS Liquid Media Supplement (Sigma, I3146). 293T cells were maintained in Dulbecco's Modified Eagle Medium (DMEM), supplemented with 10% fetal calf serum, 60 mg/ml penicillin and 100 mg/ml streptomycin. Primary hepatocytes were isolated from 6-20-week-old male h*HNF1A*$^{mut/-}$mice and cultured in Williams' E medium (GIBCO), Dexamethasone 20 ng/ml, Insulin 5mg/L, transferrin 5mg/L, 20% fetal calf serum. The culture medium was changed to complete medium with 10% fetal calf serum after 24 hours of isolation. All cells were cultured at 37°C in a humidified incubator under a 5% CO2 atmosphere.

METHOD DETAILS

Metabolic parameters and studies

Body weights were measured and recorded from 5 to 40 weeks every 5 weeks. Head and body length (between the nose and the base of tail) were measured on 40-week-old mice. For GTT and ITT, 16h (for GTT) or 4h (for ITT) fasting was performed before administration of 2g/kg glucose (for GTT) or 0.75U/kg insulin (for ITT). Blood glucose were monitored by a glucose sensor (Roche) from 0 to 120 mins every 30 mins after administration. Growth hormone and IGF-1 concentrations were examined using mouse GH and IGF-1 enzyme-linked immunosorbent assay (ELISA) kit (CUSABIO) at 10 weeks old. Mice were sacrificed after overnight fasting. The liver and body weight were recorded.

Serum total triglycerides (TG), total cholesterol (TC), low density lipoprotein (LDL), high density lipoprotein (HDL), alanine transaminase (ALT) and aspartate aminotransferase (AST) were measured by biochemistry machine (Mindray BS-830) at 20 weeks old. Serum CFD, hepatic and serum C3a levels were determined using a mouse complement factor D/adipsin ELISA kit (MULTISCIENCES) and a mouse Complement Component 3a (C3a) ELISA kit (Clond-Clone Corp.). Liver samples were used to test the hepatic TG, TC and FC levels using TG, TC and FC kit (APPLYGEN) according to the manufacturer's instructions.

Histology

Liver samples were fixed in 4% paraformaldehyde for 24h. Fixed samples were embedded in paraffin and sliced into 5μm cross sections for Hematoxylin and eosin (H&E) staining and Immunohistochemical (IHC) staining according to laboratory standard protocols to observe general morphology and HNF1α expression. Frozen samples were cut into 10μm cross sections for oil red staining to observe the fat droplets in liver samples. The primary antibodies used in the Immunohistochemical staining and the dilution ratio are provided in the key resources table.

Western blotting

Proteins were extracted from liver samples or cells with cold radioimmunoprecipitation assay buffer, then the lysates were centrifuged and collected for western blotting. The primary antibodies were used as follows: anti- HNF1α, anti-FASN, anti-SREBP-1C, anti-SCD1, anti-CD36, anti-PPARγ, anti-CFD and anti-β-ACTIN. The brands, catalog numbers and dilution ratio of the antibodies are provided in the key resources table. The membranes were visualized using AI680 (General Electric) according to the manufacturer's instructions. The gray values of the protein bands were analyzed by ImageJ software.

Quantitative real-time PCR

Total RNA was extracted from cells or tissues using TRIzol reagent. The extracted RNA was transcribed to cDNA with cDNA synthesis kit (Takara). Quantitative PCR was performed on LightCycler® 480 II (Roche) using ChamQ SYBR qPCR Master Mix (Yeasen Biotechnology). mRNA levels were determined by the comparative Cycle threshold (Ct) method (ΔΔCt) and the fold changes of each mRNA were normalized to β-actin or 36b4. Primer sequences were listed in Table S2.

Transcriptome analysis

Transcriptome analysis was performed by Novogene technology. Three liver samples from h*HNF1A*$^{-/-}$ group and four liver samples from h*HNF1A*$^{mut/-}$ group were kept in the TRIzol. Total RNA was extracted and purified. Library was prepared and its quality was detected by Agilent 2100 bioanalyzer. Sequencing was performed on machine (Illumina NovaSeq 6000). Quality was checked for raw data and fastq files were mapped to the Mus Musculus (GRCm38/mm10) reference genome using Hisat2 (v2.0.5). Three samples from each group were used for subsequent analysis. Differential expression analysis was performed using the DESeq2 R package (1.20.0). Metascape was used for GO analysis and network (http://metascape.org).[51]

Proteome analysis

Proteome analysis using TMT labelling was performed by PTM BIO technology. Each three liver samples of h*HNF1A*$^{-/-}$ and h*HNF1A*$^{mut/-}$ KI groups were kept in -80°C. Proteins were lysed and digested by trypsin. Peptides were labeled with their respective TMT reagent based on manufacturer's protocol (ThermoFisher Scientific). The samples were fractionated and the resulting peptides were used for LC-MS/MS analysis in Q ExactiveTM HF-X (ThermoFisher Scientific). The raw data were processed using MaxQuant search engine (v.1.6.15.0). Tandem mass spectra were searched against the Mus_musculus_10090_SP_20220107.fasta concatenated with reverse decoy database. The differentially expressed proteins were used to perform KEGG analysis to identify enriched pathways. The pathway with a corrected p-value < 0.05 was considered significant.

Transient transfection and FFA incubation

The coding sequence of Human *HNF1A* (GenBank: NM_001306179) was amplified by PCR using primers provided in the key resources table from human cDNA and cloned into *CMV*-Flag (Beyotime) empty vector. QuickMutation™kit of Beyotime was used to generate *CMV-HNF1A* P291fsinsC-Flag plasmid. HepG2 or AML12 cells were seeded in 6 or 12 well plates before transfection. The transfections were performed as indicated with Invitrogen Lipofectamine® 3000 Transfection Kit according to the manufacturer's instructions.

FFA solution was prepared by mixing oleic acid (OA) (Sigma, O1008) and palmitic acid (PA) (Sigma, P5585) at a mole ratio of 2:1. HepG2 cells were cultured with FFA at a final concentration of 0.2mM OA and 0.1mM PA. CFD inhibitor ACH-4471(Selleck S0803) was added to cells after 4 hours of FFA incubation at a final concentration of 0.1 or 10μM.

SiRNAs were purchased from TSINGKE Biotechnology. Two *Hnf1a* siRNAs were synthesized according to the target sequences (GenBank: NM_009327). Negative control (NC) and two siRNAs were transfected in AML12 cells according to the protocols at a final concentration of 20μM. Three *Cfd* siRNAs were synthesized according to the target sequences (GenBank: NM_001329541.1). NC and three siRNAs were transfected in primary hepatocytes of h*HNF1A*$^{mut/-}$ mice according to the protocols at a final concentration of 50μM. The sequences of siRNAs were provided in the key resources table.

Luciferase reporter assay

For luciferase reporter assay, the different lengths of human *CFD* promoter (200bp, 500bp and 1000bp) segments (GenBank: NG_007274) were inserted into PGL4.14 vector (Xitubio Biotechnology). 293T cells were plated in 24-well plate and 24h before transfection. Transient transfection was performed following the protocols. After a 30h incubation, the cells were lysed, followed by luciferase activity measurement using Promega Dual-Luciferase® Reporter Assay System.

Chromatin immunoprecipitation (ChIP) assay

HepG2 Cells with transfection of *CMV-HNF1A*-Flag plasmids were treated with 1% formaldehyde for 5 mins to crosslink DNA–protein complexes. Glycine was added to a final concentration of 125 mM for 3 mins to quench crosslinking. Cells were washed with PBS, harvested, and centrifuged at 1500rpm for 5 mins. The pellet was resuspended in ChIP lysis buffer (RIPA 0.3 buffer), and chromatin was sonicated to 200–1000 bp fragments. After short centrifugation, the cell lysis was stored at -80°C. The 1 μg anti-Flag or IgG control was incubated with beads Protein A/G (MCE) in 125 ul RIPA 0.3 buffer at 4°C for 6 hours. Then, the cell lysis was incubated with beads-antibody at 4°C overnight. The following day, Centrifuge the cell lysis-beads at 2000rpm for 1 min. Washing the beads twice with RIPA 0.3 buffer, RIPA 0 buffer, Licl buffer and TE buffer. The beads and 10 μl input were resuspended in 120μl SDS elution buffer. Reverse crosslinking was performed with the addition of RNAse A at 55°C for 1 hour, with the addition of proteinase K at 60°C for 1 hour and 65°C for 6 hours. Then, the samples were purified using TIANquick Midi Purification Kit (TIANGEN). The antibodies used for ChIP experiments (1 μg/ChIP) and primers used for qPCR were listed in the key resources table.

Primary hepatocyte isolation

The isolation of primary hepatocytes was conducted following the protocol as described previously.[52] In brief, 6-20w-old male h*HNF1A*$^{mut/-}$ mice was anesthetized and anchored. The liver was exposed and the portal vein was cannulated. After cutting the inferior vena cava, the liver became gray with continuous infusion of saline (0.5mM EDTA). Then, the solution of infusion would change to low-glucose DMEM culture medium (GIBCO) (with IV collagenase). Irrigating the surface of liver using 37°C saline. The liver became swell up and was cut into the tube with low-glucose DMEM culture medium. After filtration and washing, the primary hepatocytes were seeded into plates.

Gene correlation analysis

GEO: GSE159088 and GEO: GSE25935 profile datasets were downloaded from the GEO database (http://www.ncbi.nlm.nih.gov/geo/). The corresponding probe names were found according to the gene id and they were used for searching the expression profiles in the serious matrix data (if one gene id had more than one probe, the expression profiles were summed). The expression profiles of interested genes were used for correlation analysis in R.

QUANTIFICATION AND STATISTICAL ANALYSIS

Data were presented as mean values ± SD. The statistical analyses of the serum chemistry of mice were performed with one-way ANOVA with post-hoc comparisons using SPSS 26.0 software (IBM). All other comparisons between two groups were performed with unpaired two-tailed t-test. The comparisons among three or more than three groups were assessed with ordinary one-way ANOVA test. The statistical analyses were performed using GraphPad software (GraphPad Prism 8). All of the statistical details of experiments could be found in the figures and figure legends. A value of $p < 0.05$ was considered to be statistically significant. *$p < 0.05$; **$p < 0.01$; ***$p<0.01$; ****$p<0.0001$. The statistical methods used in this study comply with the applicable conditions required by each method.